The Characterization and Control of Shape Memory Alloy Cables for Reinforcement of Engineered Cementitious Composite Beams

A Thesis

Presented to

the Faculty of the Department of Mechanical Engineering

University of Houston

In Partial Fulfillment

of the Requirements for the Degree

Master of Science

in Mechanical Engineering

by

Xuequan Liu

December 2013

The Characterization and Control of Shape Memory Alloy Cables for Reinforcement of Engineered Cementitious Composite Beams

Xuequan Liu

Approved:

Chair of the committee
Gangbing Song, Professor
Dept. of Mechanical Engineering

Committee Members:

Li Sun, Associate Professor
Dept. of Mechanical Engineering

Mo Li, Assistant Professor
Dept. of Civil and Environment Engineering

Peng Li, Principal Technical Professional
Halliburton

Suresh K. Khator, Associate Dean
Cullen College of Engineering

Pradeep Sharma, Chair
Dept. of Mechanical Engineering

Acknowledgements

It has especially been my good fortune to have met my advisor and friends who have provided me much help during my research. They have provided me with some valuable guidance toward personal development.

Among them, I would like to acknowledge the guidance, suggestions and support provided by Dr. Gangbing Song, my advisor in research. Dr. Song introduced me to the new idea of using shape memory effect and superelasticity of a same shape memory alloy (SMA) cable to first achieve post-tensioning and then re-centering of a particular specimen. Not only did his research insight, but also his guidance outside of my research as a visionary mentor has been most invaluable during my experience at the University of Houston.

I acknowledge and appreciate committee members, Dr. Li Sun, Dr. Mo Li, and Dr. Peng Li for the facilities and support they have provided, and for making use of their valuable time to evaluate and give important comments on my thesis.

I appreciate the help from Dr. Mo Li's group, by which all the engineered cementitious composite (ECC) beams used for this study were designed and fabricated by Xiaopeng Li, as well as for the four points loading test. Dr. Li introduced me the concept of using SMA to improve the performance of ECC.

A special debt of gratitude goes to the senior students in Smart Materials and Structures Laboratory and my friends, especially Mr. Devendra Patil, Mr. Shujun Yang, and Mr. Jie Yao for helping me with the thesis. They gave me much instructions and help during this past year. I also have to thank my family for giving me the impetus to always keep moving forward with my academic and research pursuits.

The Characterization and Control of Shape Memory Alloy Cables for Reinforcement of Engineered Cementitious Composite Beams

An Abstract

of a

Thesis

Presented to

the Faculty of the Department of Mechanical Engineering

University of Houston

In Partial Fulfillment

of the Requirements for the Degree

Master of Science

in Mechanical Engineering

by

Xuequan Liu

December 2013

Abstract

This thesis reports the innovative work of improving engineered cementitious composite (ECC) beams using superelastic Nitinol shape memory alloy (SMA) cables. Nitinol is the most popularly used SMA and superelastic Nitinol cable possesses many attractive features, such as large recoverable strain, large load bearing capacity, among others. To understand the characteristics of the Nitinol cable, a series of experiments were conducted to derive its key parameters, which was not provided by the manufacturer. A sliding mode based robust controller was designed and tested to ensure the accurate force control of the Nitinol cable during the process of post-tensioning of the ECC beam. In this research, the shape memory effect of the same superelastic Nitinol cable when its temperature was below its martensite finish temperature was used to post-tensioning the ECC beam with a pre-loaded force. Experiments demonstrated that the ECC reinforced with the superelastic Nitinol cable with a pre-loaded force greatly increases the load bearing and self-repairing capacities of the ECC beam without sacrificing its ductility.

Table of Contents

List of Figures

List of Tables

Chapter 1 Introduction

Smart materials, for example, shape memory alloy (SMA), refer to the materials that are "responsive". Often the response is the conversion of one form of energy into another in useful quantities (Song, 2013). When subjected to a thermal field, SMA materials, such as Nitinol, undergo phase transformations which will produce shape changes. This thesis mainly involved the characterization and control of SMA cables for new applications in engineered cementitious composite (ECC) beams.

1.1 Problem statement and scope of this thesis

Although engineered cementitious composites (ECCs) have good ductility, the load bearing capacity is not ideal, which will narrow the potential wide applicability of ECCs. Finding a way to improve the load bearing capacity of ECC beams is still a challenge.

Nitinol, as the most popular SMA, possesses shape memory effect (SME) when its temperature is below its martensite finish temperature and superelasticity when its temperature is above its austenite finish temperature. In most reported applications of Nitinol, only one of these two properties is used. The simultaneously use of both properties of SME and superelasticity in a single application has not been reported.

Though Nitinol, in the form of cables, has the superelasticity and also large load bearing capacity, its application in ECC to increase its load bearing capacity without negatively impacting its ductility has not been reported.

This thesis intends to use superelastic Nitinol cables to reinforce ECC beams to increase its load bearing capacity through post-tensioning at room temperatures. The post-tensioning process with accurate force control is performed by using the SME of the same Nitinol cables when the environment temperature is below its martensite finish

temperature. With the pre-load force, the Nitinol cables reinforce the ECC beam at the room temperature when the Nitinol cables are in their superelastic form, which will help to increase the ECC beam's loading bearing capacity without sacrificing the ductility. Experiments will be performed to verify this.

Since the properties of the Nitinol cables are not well known from the manufacturer, experiments will be conducted to determine the key properties of the Nitinol cables. These properties will be later used for the post-tensioning of the ECC beams.

To enable an accurate force control during the post-tensioning process, a sliding mode based robust controller will be designed by taking the advantage of a previous study (Song, et al., 2000; Song, et al., 2003; Song and Ma, 2007).

1.2 Outline of the thesis

This thesis is organized as follows:

- Chapter 1 presents the organizational structure of the thesis, describes the problem statement, offers the scope of the thesis, and lists contributions of this thesis.
- Chapter 2 briefly introduces the shape memory alloy and engineered cementitious composite.
- Chapter 3 describes the characterization of the shape memory alloy cables used in this research to obtain key properties, such as the transformation temperatures, Young's modulus, and stress influenced coefficients.
- Chapter 4 applies a sliding-mode based robust controller to control force generated by shape memory alloy cables.
- Chapter 5 implements a sliding-mode based robust force controller applied to

SMA cables, which were used to post-tensioning the engineered cementitious composite beams and also act as reinforcement elements in the beams.

- Chapter 6 provides conclusions and future work related to the thesis work.

1.3 Contributions of this thesis

The main contribution of this thesis is use of Nitinol cables to reinforce an ECC beam to increase its load bearing capacity without sacrificing its ductility. The second contribution is the use of the shape memory effect of the same Nitinol cable to post-tensioning the ECC with an accurate pre-load force.

Chapter 2 Introduction to the shape memory alloy and engineered cementitious composite

2.1 Shape memory alloy

Shape memory alloys (SMAs) have the ability to return to a predetermined shape when they have been heated. When SMAs are under their transformation temperature or cold, they have very low yield strength and can be deformed very easily into a new shape, and the new shape can be retained. However, when SMAs are heated above their transformation temperature (different SMAs have different transformation temperatures, and the temperatures have a wide range from -100 to +90℃) they will return to their original shape, because when SMAs are heated, they undergo a change in crystal structure. During their phase transformation, SMAs generate an extremely large force when encountering resistance or experience a significant change in dimensions when unrestricted.

Those unique properties of SMAs make them a potentially feasible choice for actuators. SMA actuators have been used in many applications over the past decades. For example, Song and co-authors demonstrated many SMA applications in civil structures, such as SMA braces for a two-story steel frame (Song, et al., 2006). SMA actuator system for helicopter blade tab control was researched by Wu and Schetky (Wu and Schetky, 2000). Loh and co-authors described an SMA actuator design and its application in the prosthetic hand replacing conventional servo motors (Loh, et al., 2005).

When compared with other actuators, as shown in Table 2-1, it can be seen that SMA actuators offer the salient advantage, such as wide range of transformation temperatures,

more motion options (linear, torsion and bending), silent operation, and electrical and thermal control.

Table 2-1: Comparison of actuators (Song, 2013).

Types	Temperature	Motion	Characteristics
Solenoid	-50 to +120 ℃	Linear, On-Off	-Simple design -Low cost
Bimetal	-40 to +600 ℃	Bending	-Low cost -Linear response
Wax Motor	-40 to +180 ℃	Linear	-High force -Low cost -Linear response
Shape Memory	-100 to +170 ℃	Linear Torsion Bending	-High force/size -Simple design -Non-linear response -Silent operation -Electrical and thermal control

Although some SMAs have a two-way shape memory effect, research show that only SMAs with a one-way shape memory effect (SME) has good mechanical properties and only these types of SMA materials have been widely implemented, because the recovery stress of one-way SMAs is much higher than that of two-way SMAs.

There are many known alloy systems which exhibit the shape memory effect, but only several have shown promise for commercial applications, such as, Nickel-Titanium

(Nitinol), Copper-Zinc-Aluminum (Cu-Zn-Al), and Copper-Aluminum-Nickel (Cu-Al-Ni). The most popular SMA is Nitinol, and this particular alloy has very good electrical and mechanical properties, long fatigue life and high corrosion resistance (Kim, et al., 2002). As an actuator, it is capable of up to 5% strain recovery and 500 MPa restoration stress with many cycles. For example, the force generated by a Nitinol cable of 0.91 mm diameter can lift over 75 kg weights when heated. Nitinol also has resistance properties which enable it to be actuated electrically by Joule heating. From the Table 2-2, we can clearly see the high-performance properties of Nitinol.

Table 2-2: The properties of Nitinol (Song, 2013).

Nitinol cable properties	**Value**	**Unit**
Range of transformation temperatures	-100 to +90	℃
Fatigue strength	800-1000	MPa
Ultimate tensile strength	700	MPa
Admissible stress for actuator cycling	150	MPa
Electrical resistivity	80-100	10^{-8} Ω-m
Corrosion resistance	Very good	
Heat capacity	837	J/kg-℃
Thermal conductivity	18	J/m-sec-℃

SMAs can be fabricated into different shapes. This is a key factor to push them into wide applications, and the most widely used shape is SMA wire. In Figure 2-1 we can clearly see that the SMA wire possesses much more power for the same weight.

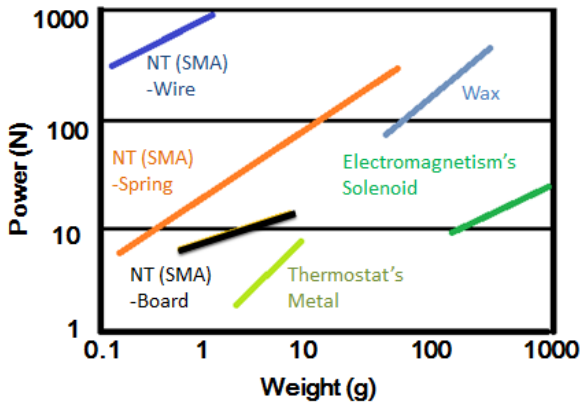

Figure 2-1: Comparison of different shape actuators (Furukawa, 2001).

When an electric current is passed directly through an SMA, heat is generated and the temperature rises, which will eventually results a phase transformation. In most cases, above room temperature is usually chosen as the transformation temperature for SMAs to use their SME. A phase transformation in their crystal structures when cooled from the stronger, high-temperature cubic form (austenite phase) to the weaker, low-temperature parallelogram form (martensite phase) makes the special properties of SMAs possible.

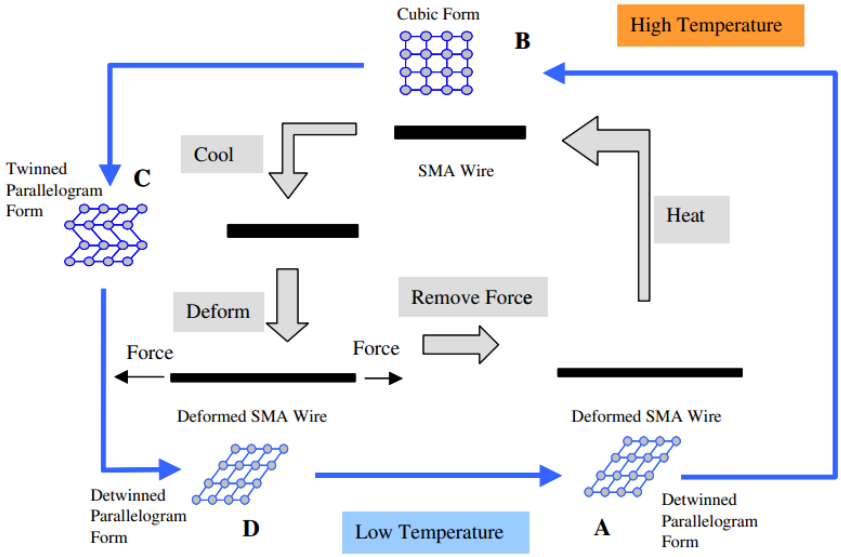

Figure 2-2: Phase transformation of SMA wire (Song, et al., 2003).

Figure 2-2 illustrates phase transformations of an SMA wire. Assume that the SMA wire is initially at a low temperature which means it is in its martensite state (as shown by point A in Figure 2-2). Upon heating, the SMA wire will experience a phase transformation to the stronger cubic austenite and the wire will contract in its length (as shown by point B in Figure 2-2). Upon cooling, the SMA wire will transfer from austenite to the weaker martensite phase (as shown by point C in Figure 2-2). At this phase, the crystal structure of the SMA is in a twinned parallelogram form. In general, its strength in terms of Young's modulus in martensite is three to six times less that in austenite (Song, et al., 2003). When an external tension force is applied to the wire, the wire can be easily stretched (as shown by point D in Figure 2-2). During this process, the twinned martensite becomes detwinned martensite upon application of an external force. When the external force is removed, the wire remains in its deformed shape (as shown by point A in Figure 2-2), and the whole cycle is complete.

Figure 2-3 depicts the length of an SMA wire versus its temperature during the phase transformation. Obviously, because the heating and cooling transformations do not overlap, the transformations exhibit a hysteretic effect. This hysteresis affects precise control of SMA actuators and may even cause the system to experience instability. Compensation of the hysteresis is a major concern during the design of control systems for SMA actuators. A method to compensate the hysteresis will be defined in Chapter 4. From Figure 2-3, we can also clearly see that there are four important temperatures, Martensite finish temperature (M_F), Martensite start temperature (M_S), Austenite start temperature (A_S), Austenite finish temperature (A_F), and their temperature relationship as shown in the Figure 2-3.

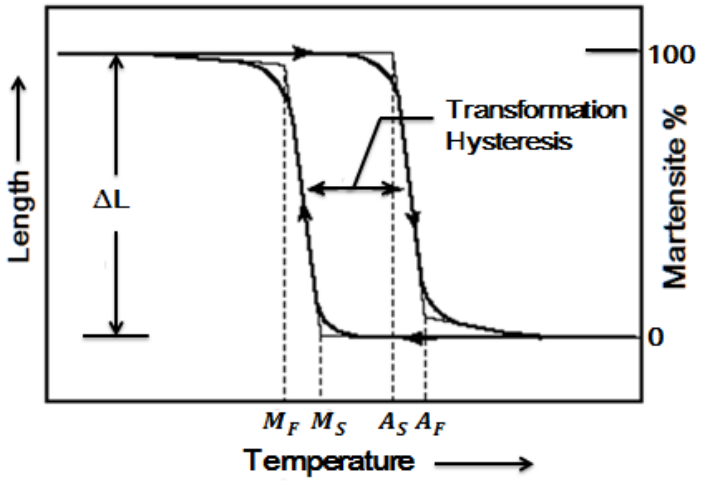

Figure 2-3: The hysteresis associated with SMA (Hodgson, et al., 2000).

There is another very important charaterstic of SMAs, the behavior of certain alloys to return to their original shape upon unloading after a substantial deformation has been applied, which is call superelasticity (Desroches, et al., 2004). The superelastic mode takes place under constant temperature conditions. When an SMA is deformed above A_F but below M_D (the temperature above which stress-induced martensite can no longer be formed), stress-induced martensite is formed. When the material is unloaded, the martensite becomes unstable and the material returns to austenite and its original shape, thus superelasticity occurs. The stress-strain curve is shown in Figure 2-4.

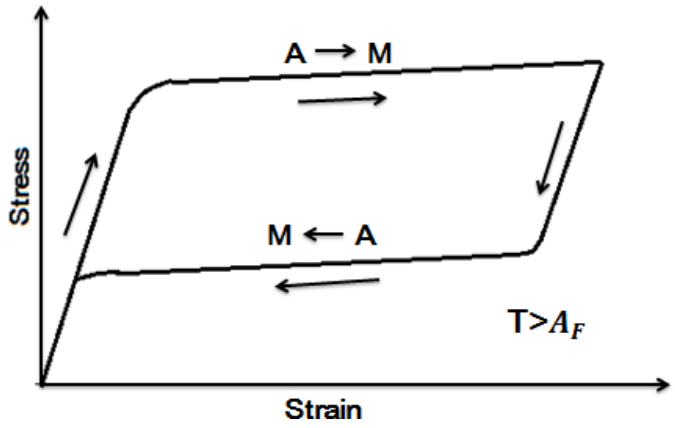

Figure 2-4: Stress and strain curve of SMA (Sreekala, et al., 2011).

The unloading curve occurs at a lower stress due to transformational hysteresis which is closely related to the thermal hysteresis in shape memory behavior. The loading plateau is the result of the martensite accommodating the applied stress by forming the crystallographic twin variant most favorably inclined to the applied stress field (Song, 2013).

2.2 Engineered cementitious composite

Engineered cementitious composite (ECC), also called bendable concrete, is an easily molded mortar-based composite reinforced with specially selected short random fibers, usually polymer fibers, with similar ingredients as fiber reinforced concrete (Li and Kanda, 1998). Various fiber types can be used in ECC, but the detailed composition must obey certain rules imposed by micromechanical considerations. This means the fiber, cementitious matrix, and the interface properties should be a correct combination in order to attain the unique feature of ECC (Li, 2013). In addition to fibers, it also contains water, cement, sand, and some common chemical additives. Coarse aggregates are not used as they tend to adversely affect the unique ductile behavior of the composite.

A number of investigations have been conducted on the applications of ECC in structural applications. These studies include the use of ECC in shear elements subjected to cyclic loading, in mechanical fuse elements in beam-column connections, in shear wall retrofitting of reinforce concreted (RC) buildings, in RC beams as durable cover for re-bar corrosion control, and in general concrete structural repair (Li and Kanda, 1998).

As we all know, traditional concrete's lack of durability and failure under strain, both stemming from brittle behavior, has been a pushing factor in the development of ECC.

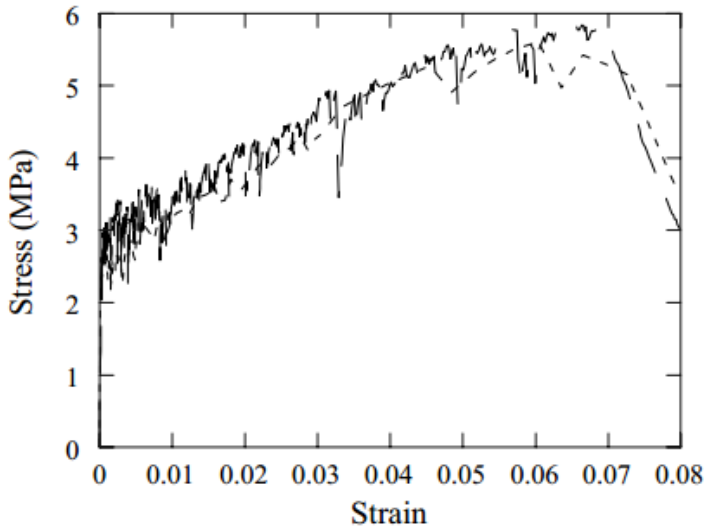

Figure 2-5: Tensile strain-hardening behavior of an ECC (Li and Kanda, 1998).

However, since ECC's load bearing capacity is not very good, it is a challenge to improve it. Advantage can be taken of ECC's strain-hardening property with Nitinol cables which act as reinforce elements, and this may be a good means of improving the load bearing capacity of the ECC.

Chapter 3 Characterization of shape memory alloys

3.1 Introduction

Shape memory alloys (SMAs) have very striking mechanical properties. To design and optimize the applications of SMAs, a clear understanding of their characteristics is required. The characteristics include transformation temperatures, Young's modulus, stress influenced coefficients at both martensite and austenite phase, damping characteristics, the potential for the generation of large internal forces, and can be changed and controlled in a precise manner. As mentioned in Chapter 2, SMAs have found many applications in various fields of civil, bio-medical, and mechanical engineering.

Unfortunately, the properties provided by the manufacturer are often not complete. Therefore, further investigation or testing needs to be conducted. Taking transformation temperatures as an example, the differential scanning calorimetry (DSC) is one of the most popular ways to determine the phase transformation temperatures. In the paper of "characterization of Cu-Al-Be shape memory alloys" DSC to determine the transformation temperatures of SMAs was used (Swamy, et al., 2012). Uchil also applied DSC to determine the transformation temperatures in the paper "shape memory alloys-characterization techniques" (Uchil, 2002). However, some researchers believe that the DSC machine is more suitable for powder form product instead of finished form product, such as cable (Choon, et al., 2007). Therefore, some other approaches should be proposed to detect the transformation temperatures. Elahinia and Ahmadian studied utilizing a linear variable differential transformer (LVDT) along with a stack of masses

applied to a SMA cable to derive the transformation temperatures (Elahinia and Ahmadian, 2005).

In this chapter, important parameters of a Nitinol cable will be measured or derived based on experimental results. For this experiment, the length of the Nitinol cable is 605 mm, the diameter is 0.91 mm, and the electrical resistivity is 71.1 milliohm-cm. The cross section of the Nitinol cable is shown in Figure 3-1. From the figure we can see the cable consists of seven wires. The diameter of a single Nitinol wire is 0.30 mm, and the electrical resistivity is 133.4 milliohm-cm. Due to its martensite finish temperature being far below the room temperature, and even reaching negative degrees Celsius in some cases, the whole test should be performed in a freezer to achieve the required temperatures.

Figure 3-1: The cross section of a Nitinol cable.

Generally, there are three different types of configurations regarding the shape memory alloy based force or pressure actuating system, as shown in Figure 3-2. In type (1), one end of the SMA cable is fixed and the other end is connected to a dead weight. The controller is relatively easier to design since the SMA cable experiences almost a constant load. In type (2), one end of the SMA cable is fixed and the other end is connected to a bias spring. When the SMA cable is heated, the cable contracts and the load on the SMA increases since the spring increases the load as the deformation of spring increases. In type (3), two ends of an SMA cable are fixed on the frame. When the

SMA cable is heated, the force will increase as the cable contracts. Among these three configurations, all of them are involved in this thesis. Sensors can be installed to read important measurements. For example, a load cell can measure the force of the SMA cable, a displacement sensor can measure the deformation of the SMA cable, and a thermal couple can measure the temperature of the SMA cable.

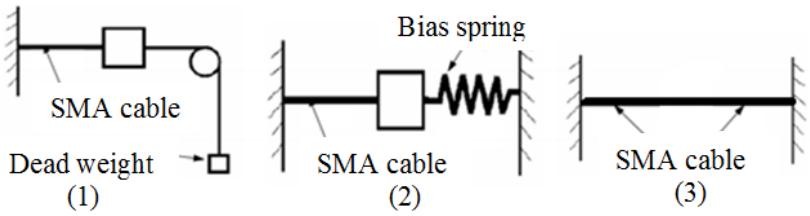

Figure 3-2: Different configurations of SMA actuating system (Li, 2011).

3.2 Experimental setup

A mechanical experimental setup, as shown in Figure 3-3, was built to provide the capability of testing the characteristic of an SMA cable. A closer look of the setup is shown in Figure 3-4. This design configuration is adopted in the SMA test frame. In this SMA test frame, one end of the SMA cable is fixed on the frame, while the other end is connected to an insulator. The insulator is connected to a load cell and the load cell is connected to a biased spring. A displacement sensor and a thermal couple are also installed on the frame to measure the deformation and the variation of temperature of the SMA cable, respectively. When the SMA cable is heated through an electrical current, the load on the SMA increases, as the cable contracts, and the spring increases the load as its deformation of the spring increases.

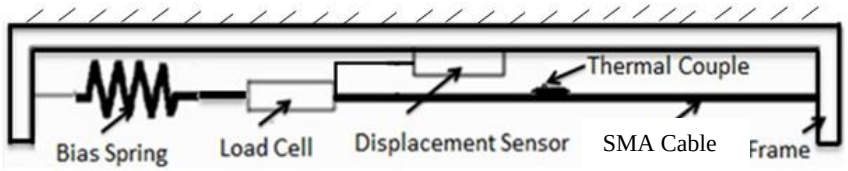

Figure 3-3: Mechanical setup.

The spring coefficient was characterized by the relationship between the applied dead weights and the measured displacement, and it was found to be 0.76 N/mm.

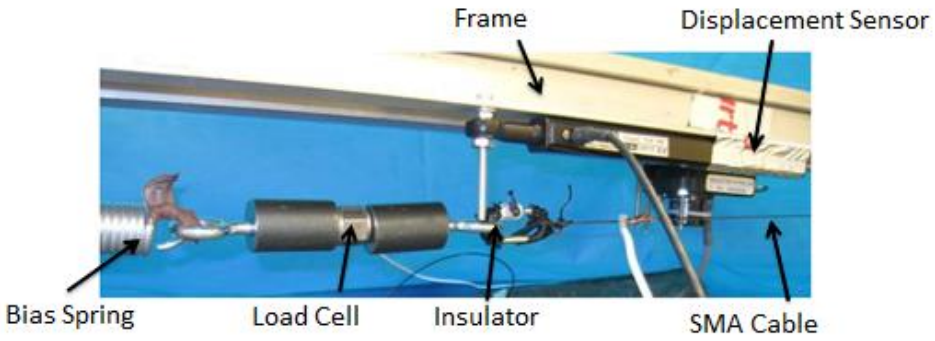

Figure 3-4: A closer look of the setup.

The SMA's force and deformation results from experiment are shown in Figures 3-5 and 3-6. It can be seen that the SMA cable reached the target deformation (23 mm) within 18 seconds, but the process of cooling took a much longer time. This is because the rate of cooling is slower. Based on the Figures 3-5 and 3-6, the force-displacement relationship is plotted. From the Figure 3-7, it is also shown that the coefficient of the spring is 0.76 N/mm.

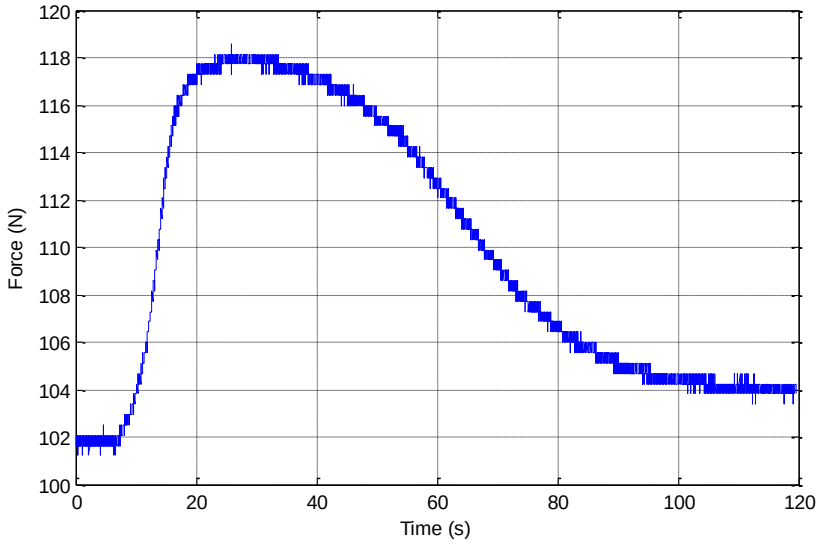

Figure 3-5: Force variation of SMA cable versus time.

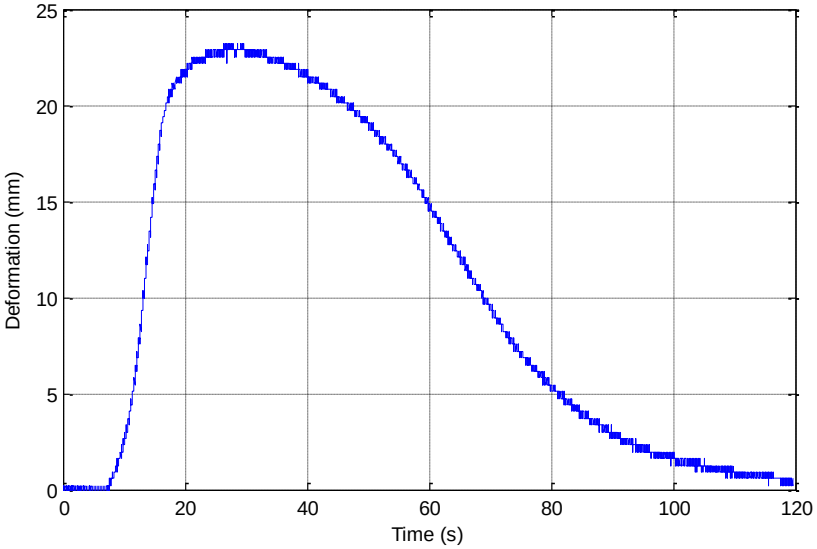

Figure 3-6: Deformation of SMA cable versus time.

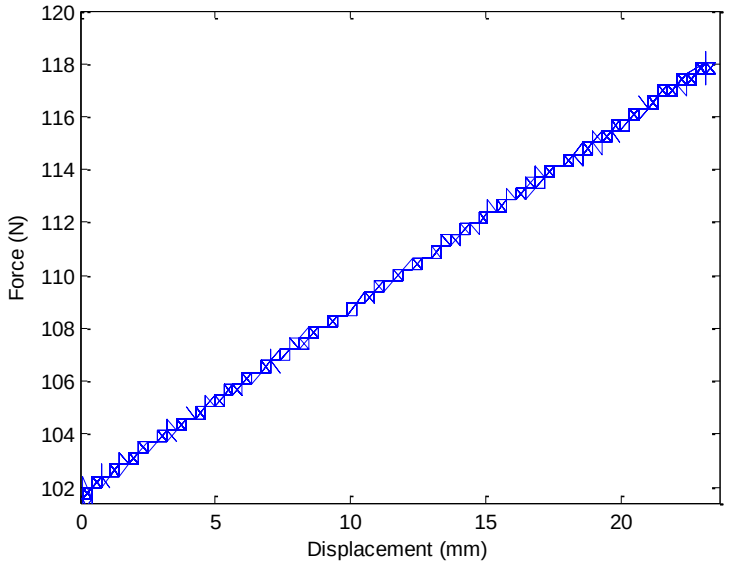

Figure 3-7: Force versus displacement response of the spring.

3.3 Protection of the SMA cable

The SMA cable requires protection against damage because of overloading, excessive deformation, or overheating, all of which will contribute to permanent failure of the SMA cable. Several protection measures will be proposed in this thesis.

3.3.1 Excessive deformation protection

In order to prevent the SMA cable from excessive deformation, a protection measure becomes particularly important. When the deformation increases to over 5 percent of the entire length of the SMA cable, the heating of the cable will be stopped. Below is the designed protection, as shown in Figure 3-8. Digital analog converter (DAC) connected to a power supply is used to drive the SMA cables.

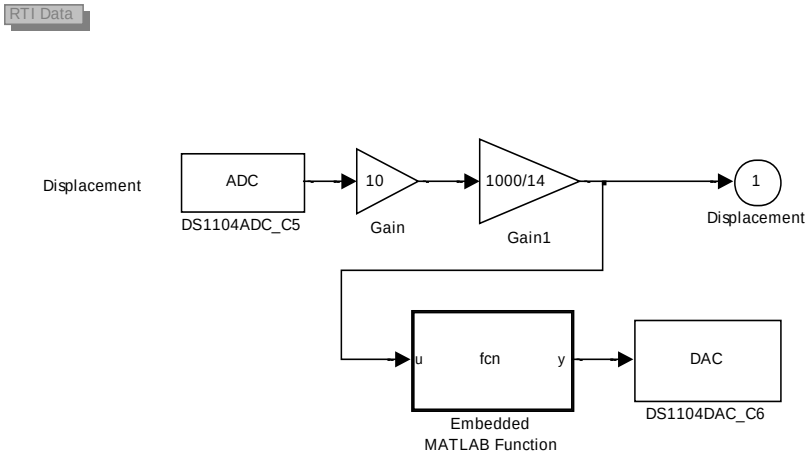

Figure 3-8: Block diagram of excessive deformation protection.

3.3.2 Excessive force protection

In order to prevent the SMA cable from overloading, a force protector is a necessary addition to the system. When the applied force exceeds 200 N, the heating will be stopped. Below is the protector, as shown in Figure 3-9.

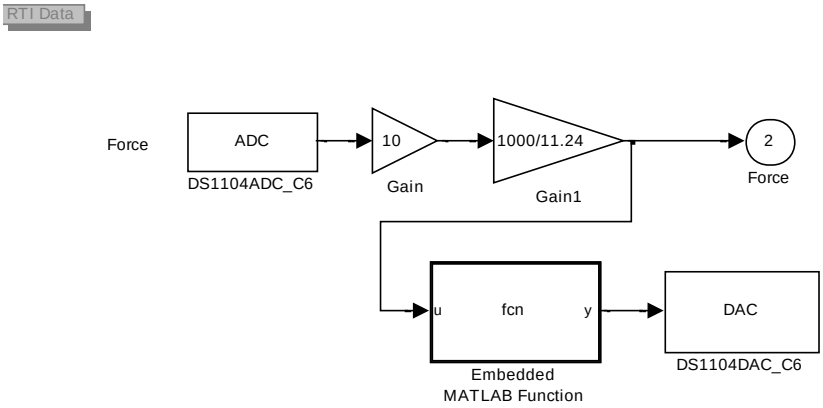

Figure 3-9: Block diagram of excessive force protection.

3.3.3 Overheating protection

In order to prevent the SMA cable from overheating, a measure is designed. When the temperature reaches 50 ℃, the heating of the cable will be stopped. The Figure 3-10 shows the overheating protection.

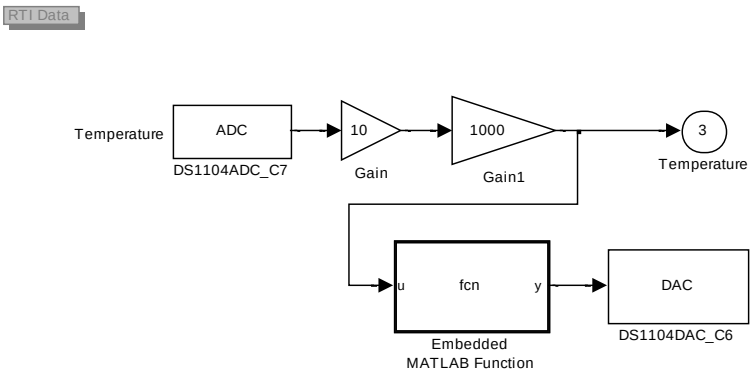

Figure 3-10: Block diagram of the overheating protection.

3.4 Experimental testing

Configuration type one was used to test the characteristics of the SMA cable. One end of the SMA cable is fixed on the frame, while other end is connected to the load cell. The dead weight hung through the load cell and thermal couples were installed to detect the temperature of the cable. A closer look at the configuration type one is shown in Figure 3-11. The diameter of the SMA cable was around 0.91mm. After being fixed on the frame, the length was about 605 mm. It was fixed between a dead weight and the frame.

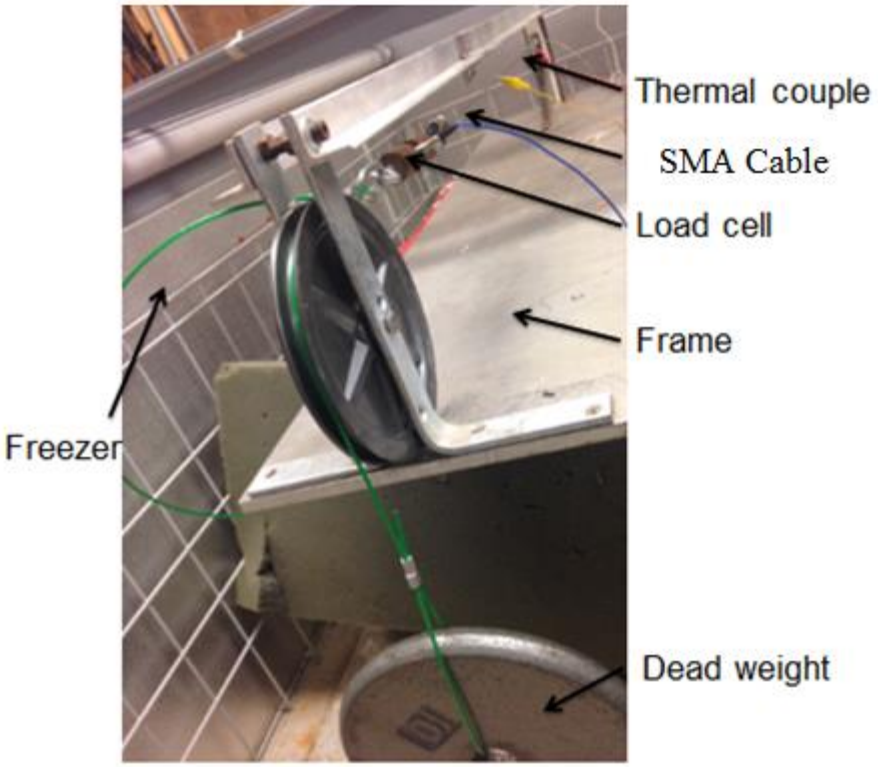

Figure 3-11: A closer look at configuration type (1).

3.4.1 Phase transformation temperatures for the SMA cable

The purpose of the experimental measurements is to establish the values of the start (S) and finish (F) transformation temperatures from the martensite (M) to austenite (A) phase of the SMA cable. Since the transformation temperatures depend on the stress, four different stress levels are applied to the SMA cable. The stress applied to the SMA cable can be adjusted by adding or removing dead weights from the stack. There are four dead weights of 20, 35, 45, and 65 pounds (the corresponding system international value is 9, 16, 20, and 29 kg, respectively), which were applied throughout the tests. The SMA cable was heated by the power supply. During each test, changes in the length of the cable, the temperature, and deformation of the cable were precisely observed and measured. For each load level, a set of four characteristic transformation temperatures of the cable were found, as shown from Figures 3-16 to 3-19. Then, using a simple algorithm, the values of

the characteristic transformation temperatures of M_S, M_F, A_S, and A_F of the cable at "zero" stress conditions were obtained (Zak, et al., 2003). In order to have a relatively accurate result, the weight of the cables used to hang the dead weight and the screw used to fix the cable have also been taken into account in this analysis. Typical results from the tests are presented in Figure 3-15.

The low temperature in the freezer requires appropriate driving voltage to heat the SMA cable. In order to get better cures for the transformation temperatures, application of a real time system through dSPACE to heat the SMA cable has been proposed. The real time system was designed, as shown in Figure 3-12. This approach is to realize a gradual increase in the voltage. Every five seconds, an increase of 1Volt (V) was applied. Once the maximum voltage was achieved, the voltage was decreased by 1V every 5 seconds. The output heat voltage is shown in Figure 3-13.

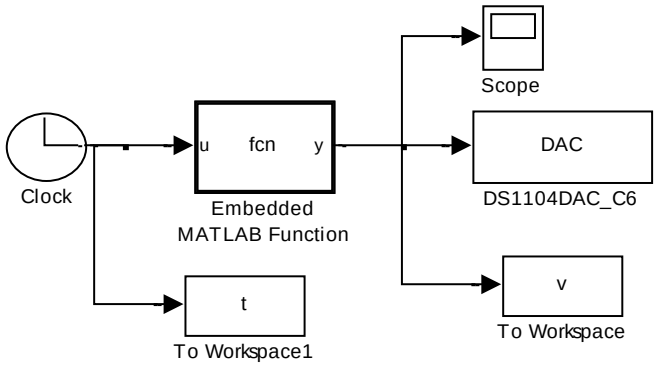

Figure 3-12: Block diagram of heating voltage control program.

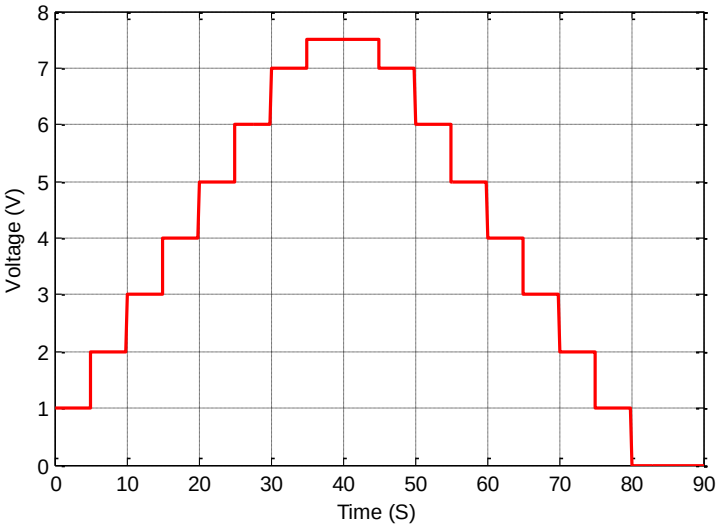

Figure 3-13: Applied voltage profile.

Before using the approach, heat may be lost because of the cool air of the freezer. Below is a comparison of the results obtained by using the approach, as Figures 3-14 (with this approach) and 3-15 show (without this approach).

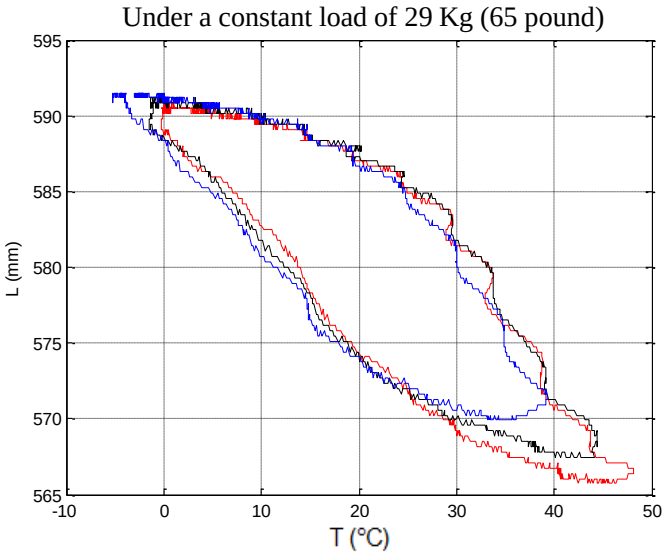

Figure 3-14: The SMA cable length versus temperature at 29 kg load level.

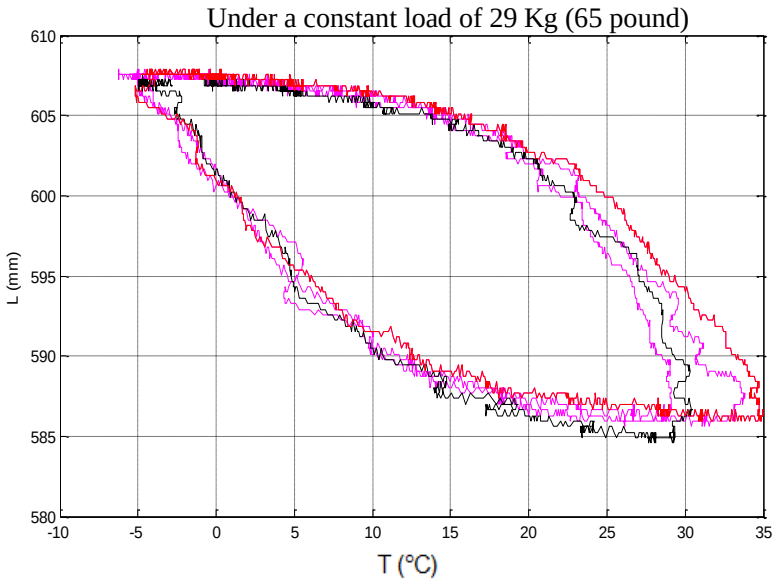

Figure 3-15: The SMA cable length versus temperature at 29 kg load level.

In order to achieve accurate and precise results, tests were repeated, and the different loops stand for different cycles at the same constant load. From the results we can clearly see that every cycle does not overlap. This is because the ambient temperature varies with time. This may be especially prevalent in the freezer as the freezer may dissipate the heat applied to the SMA cable.

The experimental results of the same procedure at four different stresses are shown in Figures 3-16 to 3-19. The SMA cable at different stress levels have different transformation temperatures and the recovery strain is also different. The larger the applied stress value to the SMA cable, the higher the transformation temperatures will be. Only one of the widest cycles is chosen for further analysis. In order to better capture this feature, a filter is necessary. The data processed by a low pass filter are shown in Figures 3-20 to 3-23.

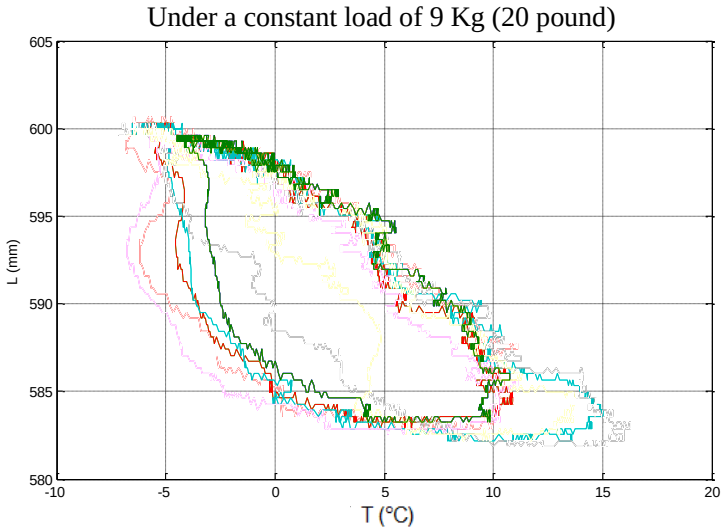

Figure 3-16: A typical curve for changes in the length of the SMA cable as a function of temperature during heating and cooling at a constant 9 kg load level.

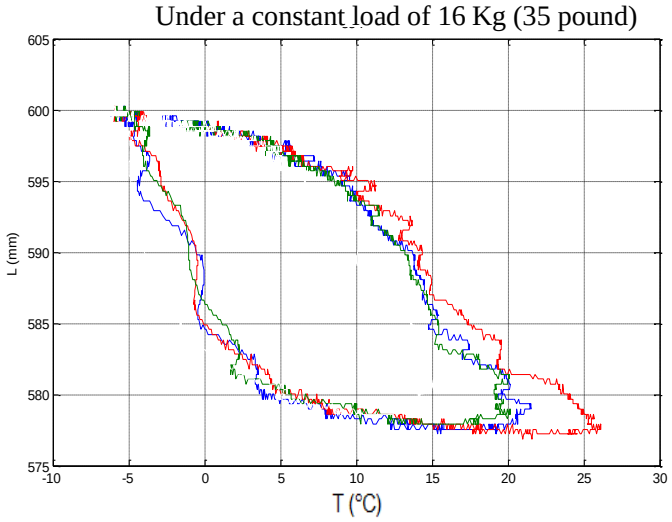

Figure 3-17: A typical curve for changes in the length of the SMA cable as a function of temperature during heating and cooling at a constant 16 kg load level.

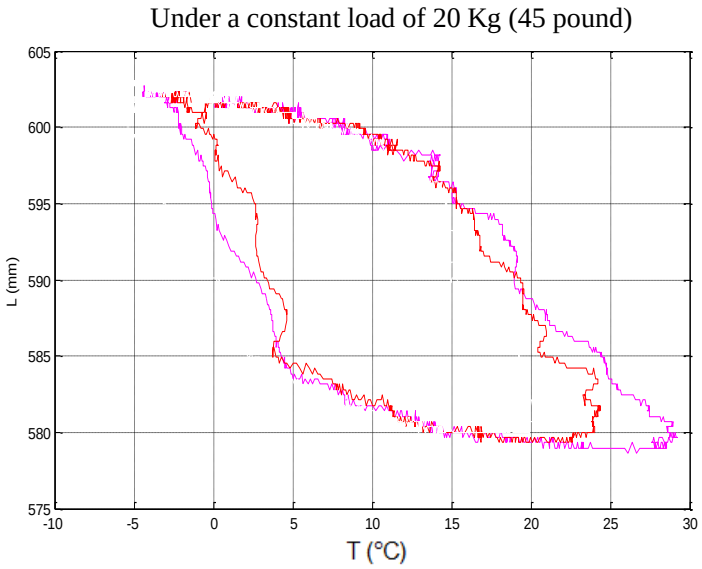

Figure 3-18: A typical curve for changes in the length of the SMA cable as a function of temperature during heating and cooling at a constant 20 kg load level.

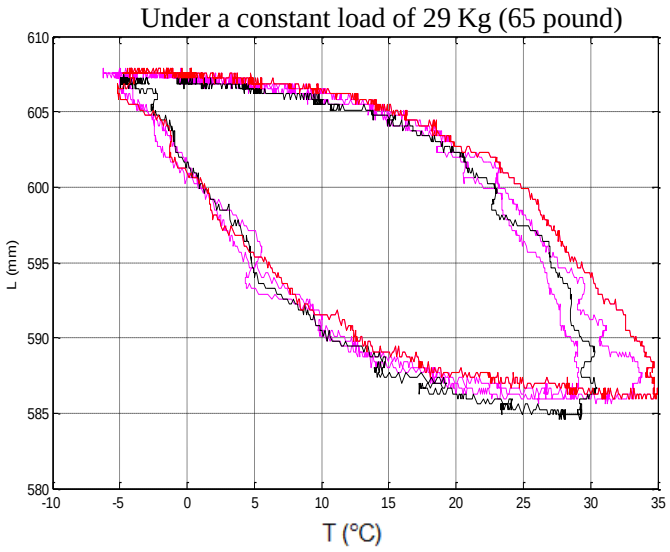

Figure 3-19: A typical curve for changes in the length of the SMA cable as a function of temperature during heating and cooling at a constant 29 kg load level.

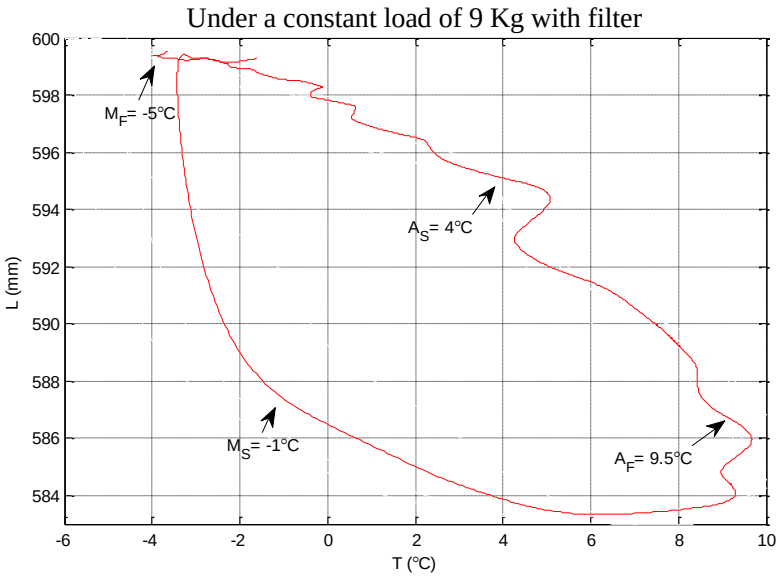

Figure 3-20: A typical curve for changes in the length of the SMA cable as a function of temperature during heating and cooling at a constant of 9 kg load level with filter.

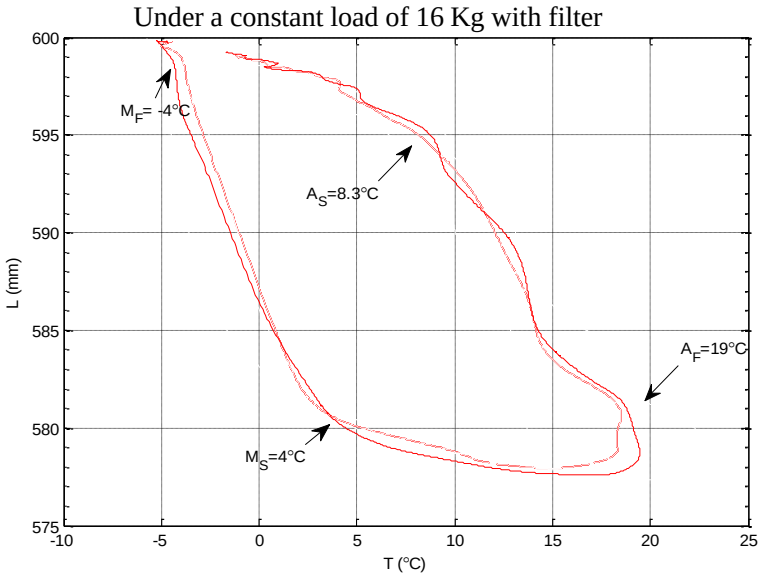

Figure 3-21: A typical curve for changes in the length of the SMA cable as a function of temperature during heating and cooling at a constant of 16 kg load level with filter.

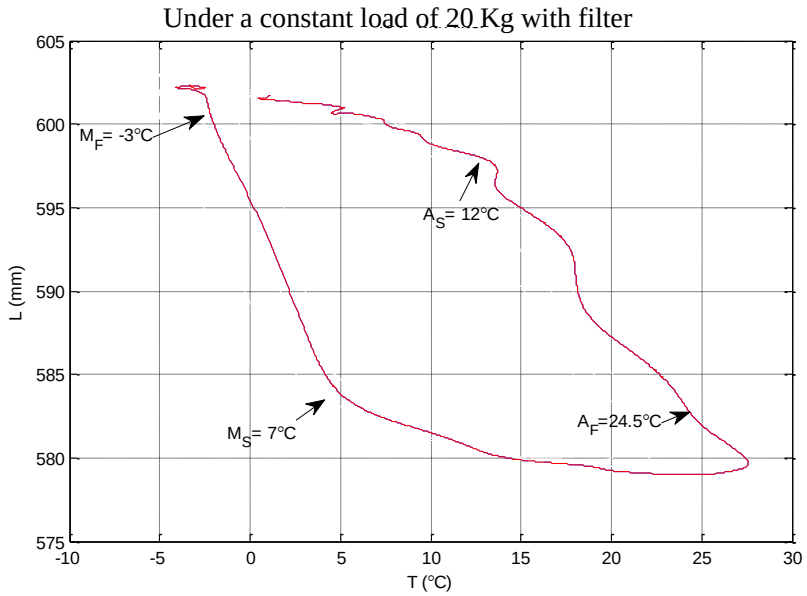

Figure 3-22: A typical curve for changes in the length of the SMA cable as a function of temperature during heating and cooling at a constant of 20 kg load level with filter.

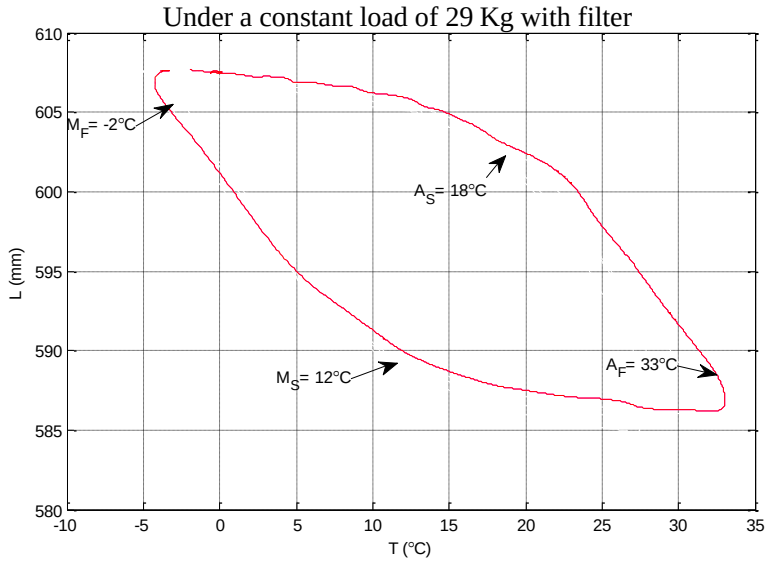

Figure 3-23: A typical curve for changes in the length of the SMA cable as a function of temperature during heating and cooling at a constant of 29 kg load level with filter.

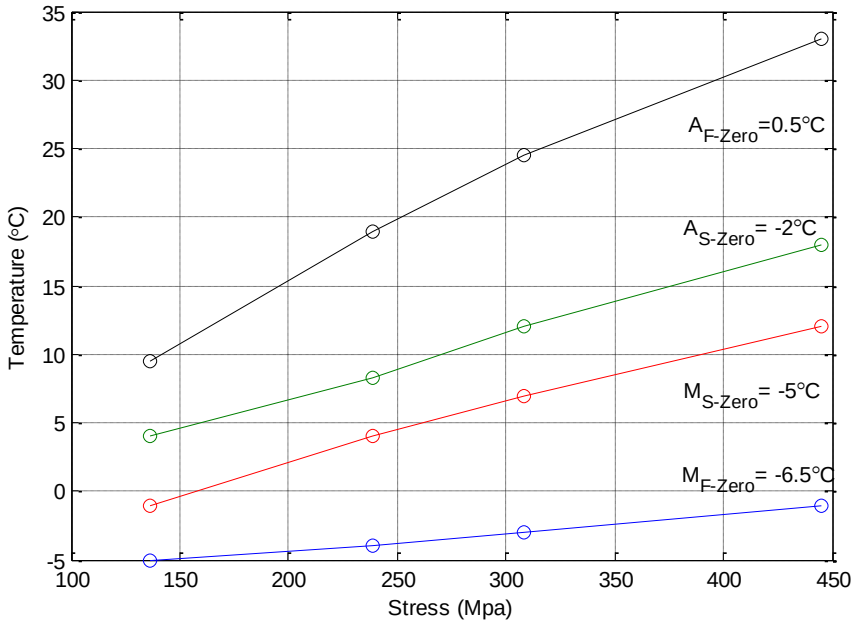

Figure 3-24: Temperature-stress characteristics for the characteristic transformation temperatures of the SMA cable.

The temperature–stress characteristics of the SMA cable can be established from plotting the values of the characteristic transformation temperatures, and those temperatures can be obtained from the results presented in above figures. As a result, the four lines indicating changes in the characteristic transformation temperatures M_S, M_F, A_S, and A_F of the SMA cable for varying stress value are obtained, as shown in Figure 3-24. Therefore, the values of the characteristic transformation temperatures of the SMA cables, at "zero" stress conditions, can easily be found by linear extrapolation from the known levels of stresses to "zero" stress conditions (Zak, et al., 2003). In Figure 3-24, the values of the characteristic transformation temperatures of the SMA cable corresponding to "zero" stress conditions are also shown.

As mentioned earlier, there are four different constant loads applied to the SMA cable, and the force over temperature results are shown in Figures 3-25 to 3-28. From these results, we can also conclude that the SMA cable has severe hysteresis.

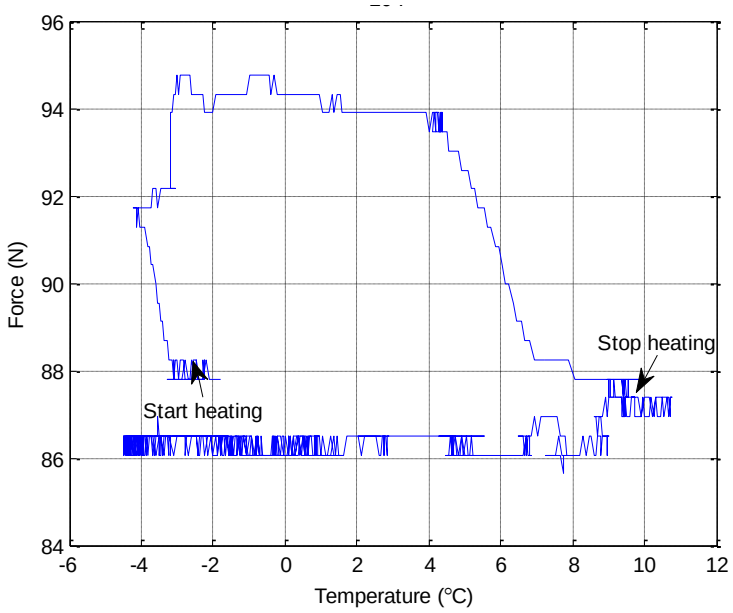

Figure 3-25: Force over temperature under a constant load of 9 kg.

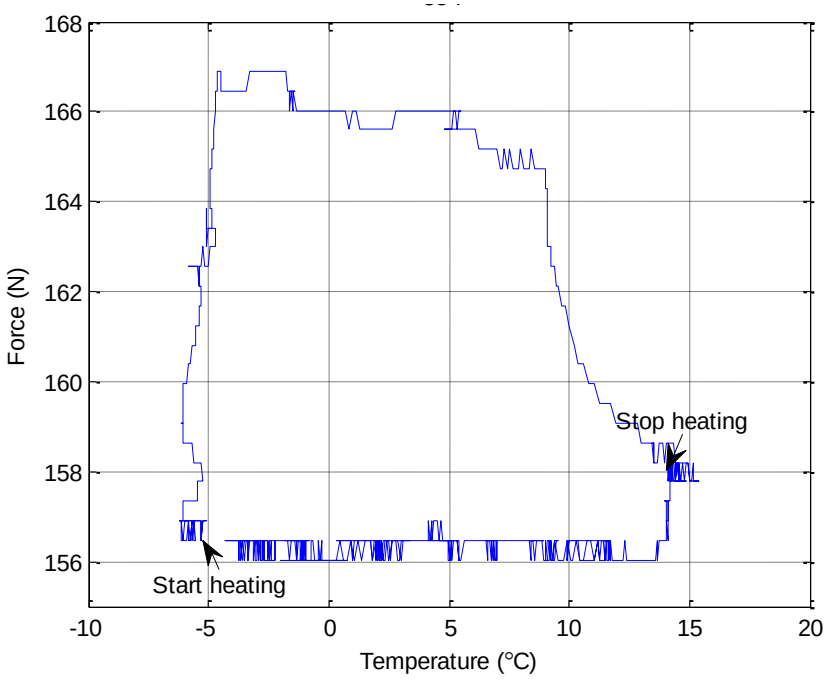

Figure 3-26: Force over temperature under a constant load of 16 kg.

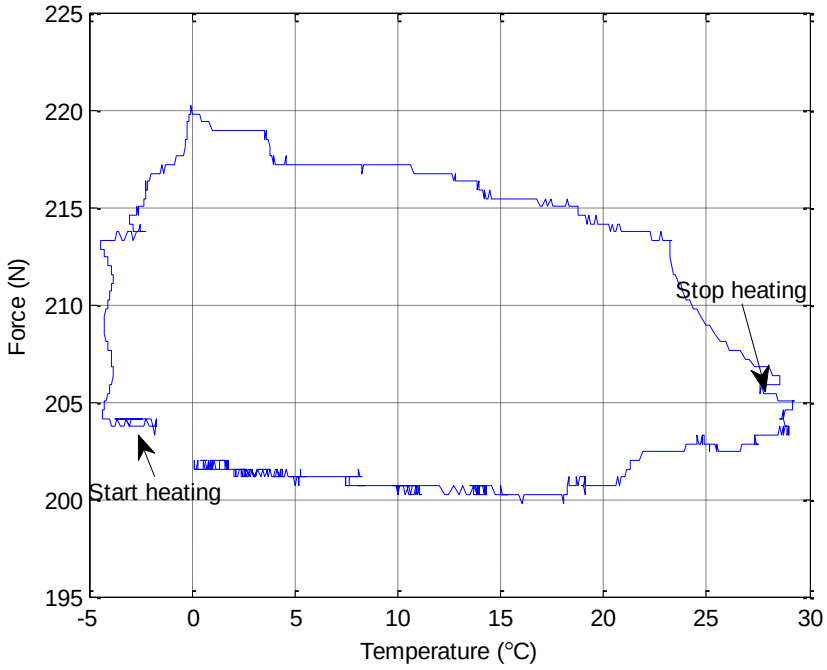

Figure 3-27: Force over temperature under a constant load of 20 kg.

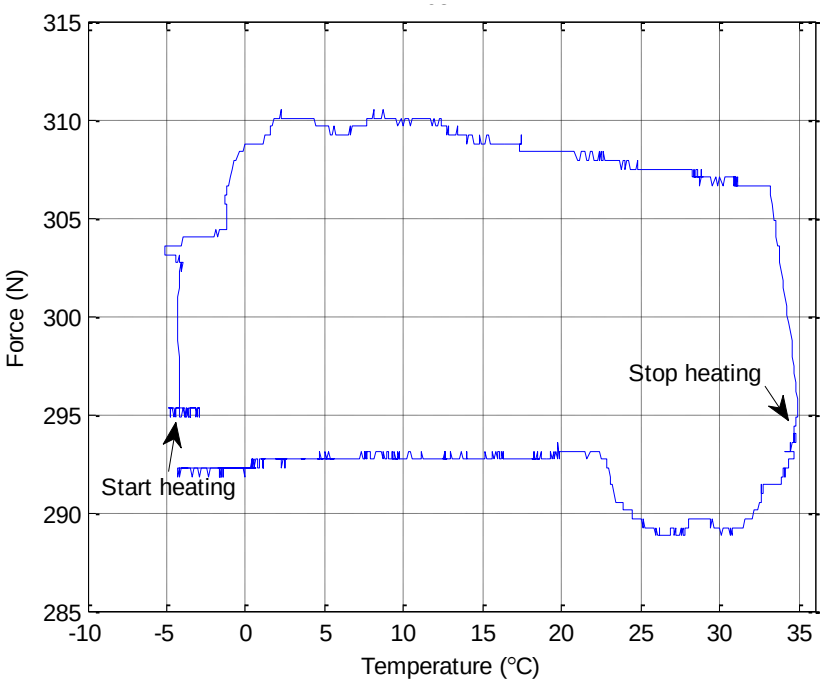

Figure 3-28: Force over temperature under a constant load of 29 kg.

3.4.2 Young's modulus and stress influenced coefficients

There are other thermo-mechanical properties of the SMA cable were investigated in this section. The process of loading and unloading of the cable at a constant temperature can be performed to obtain stress-strain curves. The force and the deformation of the SMA cable were measured during the entire process. The Young's modulus of the austenite phase (E_A) and martensite phases (E_M), could be obtained as well. In addition, values of the critical stresses for the start of the transformation from austenite to martensite (σ_{AM}), as well as the start of the transformation from martensite to austenite (σ_{MA}) can be found, as presented in Figure 3-29.

In order to find values of the stress influenced coefficients at martensite phase $(\mathrm{C_M})$ and austenite phase $(\mathrm{C_A})$, and the values of the critical stresses σ_{AM} and σ_{MA}, the loading and unloading of the SMA cable at different temperature levels were used. It is worth mentioning that, due to the process of uncontrolled cooling of the cable, in each measurement the temperature of the cable may be different during the process of loading and unloading. In addition, the electrical resistance of the SMA wires varies intrinsically as the material undergoes a phase change between martensite and austenite (Kotil, et al., 2003).

Since each test was carried out at a constant voltage level, the electrical power was affected by changes in the resistivity of the cable during the transformations, and thus changes in the temperature of the cable were expected and observed (Zak, et al., 2003). These changes in the temperature of the cable were measured during the tests.

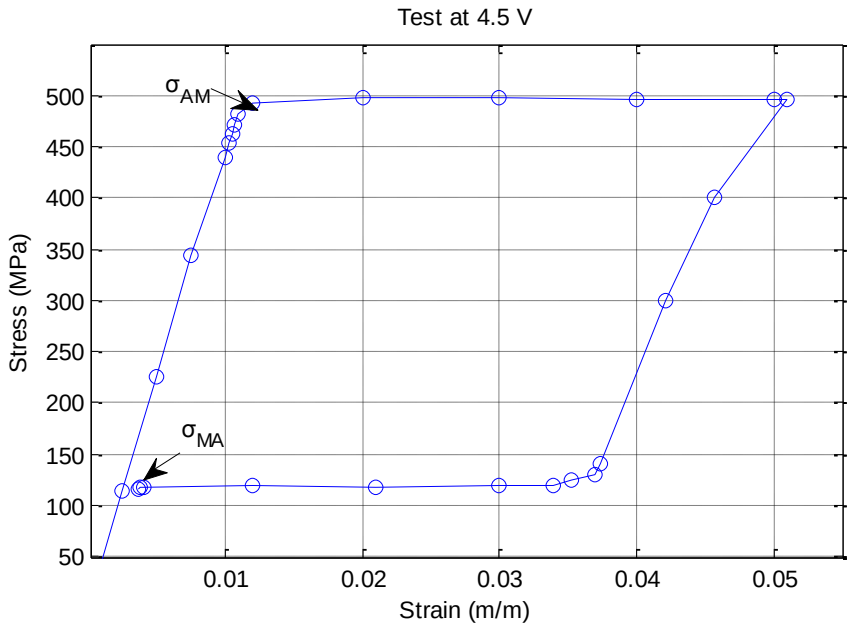

Figure 3-29: A typical loading and unloading curve of the SMA cable.

In order to determine the Young's modulus respectively for the martensite and austenite phases of the SMA cable, loading and unloading tests for the cable were carried out. The results obtained from the tests were presented in Figure 3-30. At a constant temperature the loading test was performed for the cable in the austenite phase. Similarly, at a constant temperature the loading and unloading test for the martensite phase was carried out.

The loading and unloading tests of the cable were carried out for constant voltage levels of 4.0, 4.5, and 5.0 V. From the results, the values of the critical stresses for the start of the transformation from austenite to martensite σ_{AM} were determined as a function of temperature of the cable (Zak, et al., 2003). Similarly, the values of the critical stress for the start of the transformation from martensite to austenite σ_{MA} were obtained throughout the same tests. The results obtained were presented in Table 3-1. Using the results from Table 3-1, the stress influenced coefficients C_M and C_A of the

cable can be easily found. Since the measured values were not in the same straight line, through approximation, the slopes of the approximating straight lines can be seen in Figure 3-31.

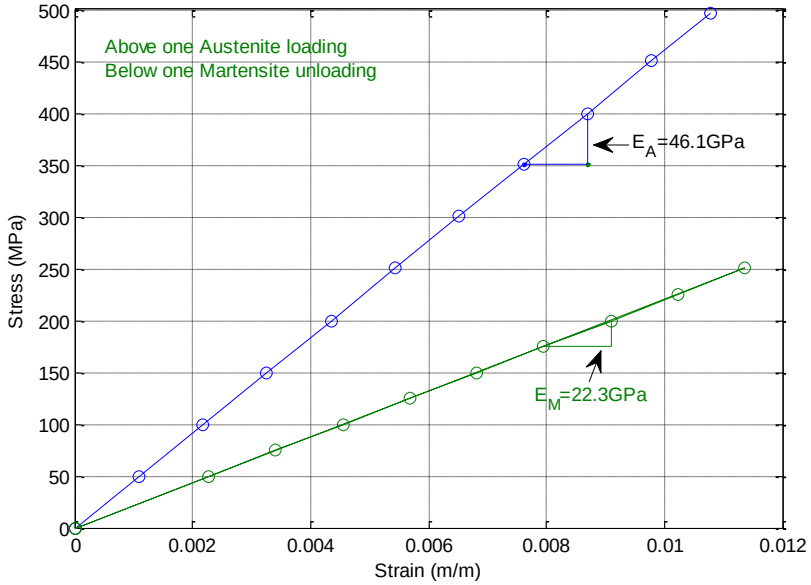

Figure 3-30: Young's modulus of both martensite and austenite phases of the SMA cable.

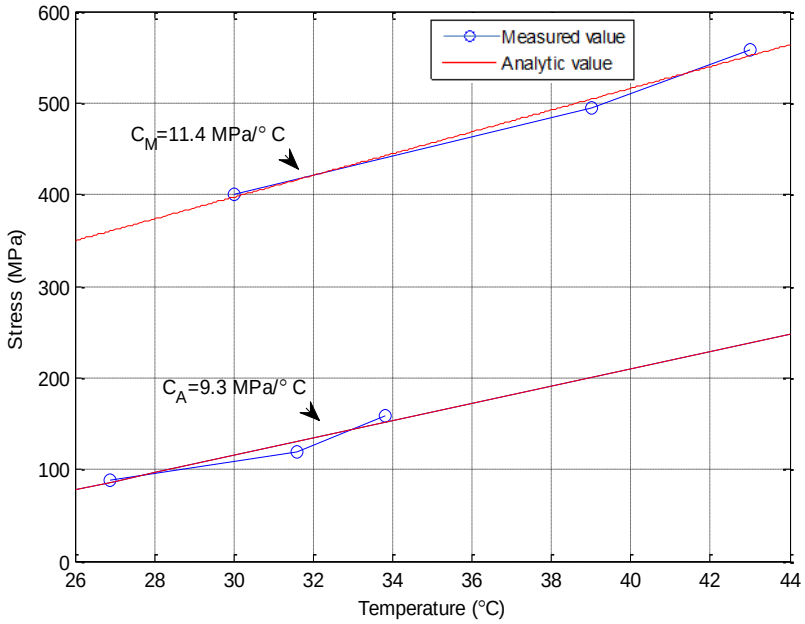

Figure 3-31: Stress influenced coefficients C_M and C_A of the cable.

3.5 Experimental results

Table 3-1: Values of the critical stress of the SMA cable and corresponding temperatures.

Voltage (V)	**Critical stress σ_{AM} (MPa)**	**Temperature At σ_{AM}(℃)**	**Critical stress σ_{MA} (MPa)**	**Temperature At σ_{MA}(℃)**
4	400	30	89	24.2
4.5	495	39	120	31.6
5	558	43	158	33.8

Table 3-2: Material properties of the SMA cable.

Property	**Value**
Martensite finish temperature M_F (℃)	-6.5
Martensite start temperature M_S (℃)	-5
Austenite start temperature A_S (℃)	-2
Austenite finish temperature A_F (℃)	0.5
Stress influenced coefficient C_M (MPa/℃)	9.3
Stress influenced coefficient C_A (MPa/℃)	11.4
Young's modulus E_M (GPa)	22.3
Young's modulus E_A (GPa)	46.1

From Table 3-1 and Table 3-2, key parameters of the SMA can be clearly seen. Regarding the transformation temperatures of the SMA cable, the austenite starts at -2 ℃ and finishes at 0.5 ℃, while the martensite starts at -5 ℃ and finished at -6.5 ℃.

Furthermore, the larger the stress applied to the SMA cable, the higher the transformation temperatures of the SMA cable will be. The Young's modulus of the SMA at the martensite phase is 22.3 GPa, while 46.1 GPa is the value at the austenite phase, which means SMA has a higher Young's modulus in the austenite phase than in its martensite phase. The stress influenced coefficient at the martensite state is 9.3 MPa/℃, while one of the austenite state is 11.4 MPa/℃.

3.6 Summary

In this chapter, a series of experiments were conducted to derive the SMA cable's key parameters, which were not provided by the manufacturer. These parameters will assist us to reinforce the ECC using the SMA cables in a later chapter. From the experimental results, severe hysteresis associated with SMAs can be observed. In the following chapter an approach will be adopted from a previous research to compensate for the hysteresis to achieve accurate force control of the SMA cable.

Chapter 4 Robust force tracking control of shape memory alloy cables

4.1 Introduction

Tracking control of shape memory alloy (SMA) actuators is very important in many applications, such as aircraft wing controls, vibration control, robotic and civil engineering applications. However, due to hysteresis, an inherent nonlinear phenomenon associated with SMAs, tracking control of SMA actuators is always a challenging task. This has motivated many authors to conduct research in tracking control of SMA actuators with hysteresis compensation.

Many different methods have been proposed to compensate the hysteresis for tracking control of SMAs. Ma and Song studied internal electrical resistance feedback using neural networks for position control of SMAs (Ma and Song, 2004). Hysteresis compensation for SMA actuators using a fuzzy logic based inverse Preisach model was presented by Nguyen (Nguyen, et al., 2007). Tracking control of SMA actuators based on self-sensing feedback and inverse hysteresis compensation was carried out (Liu, et al., 2010).

In this chapter, a sliding-mode based robust controller will be applied to the tracking control of the force generated by an SMA cable. Due to fact that the temperatures in the freezer were unsteady, tracking of the force can be affected. In this chapter, a feedforward controller was used to reduce the hysteresis. A sliding-mode based robust controller was used to compensate uncertainties such as the error in hysteresis cancellation and to ensure system stability (Song and Ma, 2007). Experiments have been

conducted and showed that the measured force of the actuator can closely followed that of the desired reference.

4.2 Experimental setup

A mechanical experimental setup as shown in Figure 4-1 was built to provide the capability of testing and force feedback control of an SMA cable. This design configuration was adopted in the SMA test frame. In this SMA test frame, the two ends of the SMA cable were fixed on the frame. One end of the cable was fixed on the frame through a hook. The other end was connected to the load cell and the load cell was fixed on the frame as well. The load cell was used to measure the force generated by the SMA cable. This force was then fed back to the real-time control system.

Control systems can be defined and implemented using dSPACE data acquisition and a real-time control system with Matlab/Simulink as shown in Figure 4-1. An output voltage from the real-time control system was sent to a programmable power supply. In this chapter, the power supply was set in constant-voltage control mode. The power supply amplifies the voltage by a factor of four and then applies the amplified voltage to the SMA cable, which results in a direct current in the SMA and in turn heats the SMA cable.

The heating of the cable above the transformation temperature of austenite causes a phase transformation from the pliable martensite to the rigid austenite, which as can be seen by the SMA cable contraction, the force increases. Once the voltage is cut off and the heat is removed from the SMA cable, the temperature of the freezer will revert the SMA cable into the martensite phase. The cable will experience a phase transformation

from austenite back to martensite. The weak martensite phase has low yield strengths, the cable will loosen, and the force will drop. An actuation cycle is completed.

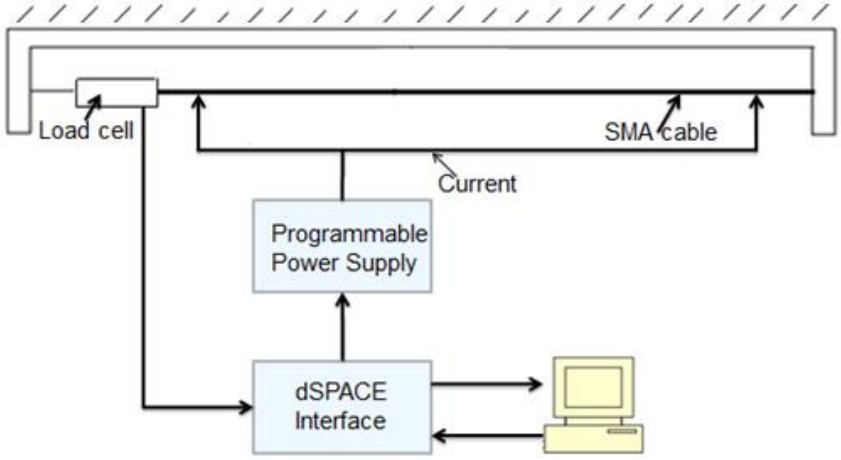

Figure 4-1: Overall setup for the force controller.

4.3 Control system design

From Figure 4-2, feedforward and feedback parts can be clearly recognized in the defined controller. The feedforward part was defined to considerably reduce the hysteretic effect. The feedback part includes a linear proportional derivative (PD) control and a nonlinear sliding-mode based robust controller. The robust controller was defined to compensate the residual hysteresis and other nonlinearities to ensure the system's stability (Song, et al., 2003).

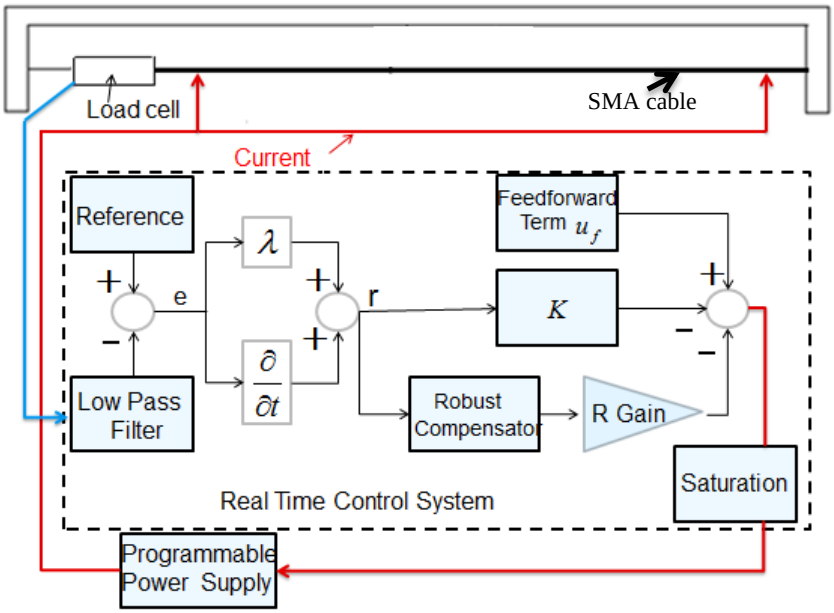

Figure 4-2: The block diagram of the control system.

In order to better understand the feedback control defined, the control errors have been defined as

$$e = y - y^d,\ \dot{e} = \dot{y} - \dot{y}^d, \qquad (4\text{-}1)$$

where y and y^d are the desired force output and measured force output, respectively. Also we define auxiliary control variables r and $\dot{r}$ by

$$r = \dot{e} + \lambda e,\ \dot{r} = \ddot{e} + \lambda \dot{e}, \qquad (4\text{-}2)$$

the coefficient λ is a positive constant and r = constant means a surface in phase space. The surface defined by r = 0 represents the "sliding surface", so that, when the dynamics are restricted to this surface, e = 0 and $\dot{e} = 0$ is an asymptotically stable equilibrium point with a global basin of attraction (within r = 0). Therefore, when the system is restricted to the sliding surface, the control errors diminish as t reaches to infinity (Song, et al., 2003).

Utilizing the auxiliary control variable r, the force tracking controller was conducted

as

$$F = u_f - Kr - \rho tanh(\alpha r), \qquad (4\text{-}3)$$

where K and α are positive constants. The functions of each control part in equation 4-3 are explained as follows.

Firstly, the u_f is a feedforward voltage and was defined to provide the approximate amount of voltage required for the SMA cable to follow the desired reference which was used for the significant reduction of the hysteresis of the SMA cable. The constant value u_f was determined by experiments (Song, et al., 2000).

Secondly, the $-Kr$ part of the equation is a linear feedback part functioning as a PD control. Proportional control was used to decrease steady-state error and increase responsiveness of the SMA cable. The derivative control was used to increase damping and to stabilize the SMA cable. In the experiment, an appropriate value of the P gain ($-K r \lambda$) has to be used since a large value may cause overshot oscillations and a small value may result in larger steady state error and a slower response (Song and Ma, 2007).

Thirdly, the $-\rho \tanh(\alpha r)$ is a sliding-mode based robust compensator and was used to compensate for the hysteresis of the SMA cable and to increase control accuracy and stability. The control parameter ρ was an estimated upper bound on the residual hysteresis and other nonlinearities associated with the SMA system. In this chapter, ρ is also called robust (R) gain. The constant α determined local gain near the origin when r was very small, therefore, a larger value of α results in a smaller steady state error. However, a larger value of α also has a greater tendency to excite the flexible mode of the system. The value of α will be experimentally determined by considering the above factors (Song, et al., 2003).

A block diagram used to demonstrate the control system as shown in Figure 4-2. In order to achieve higher accuracy and avoid aliasing, a low-pass analog Butterworth filter with a cut-off frequency of 30 rads/sec was used to filter out high-frequency noise in the signal from the load cell. The sampling rate was 1000 Hz. The 8th order transfer function of the low-pass filter was presented as shown in Table 4-1, and the corresponding bode plot as shown in Figure 4-3.

Table 4-1: Coefficients for 8th order Butterworth filter.

Order	Numerator	Denominator
0	2.347×10^{-15}	1
1	$1.878\times10^{-14}Z^{-1}$	$-7.846\times Z^{-1}$
2	$6.572\times10^{-14}Z^{-2}$	$26.94\times Z^{-2}$
3	$1.314\times10^{-13}Z^{-3}$	$-52.84\times Z^{-3}$
4	$1.643\times10^{-13}Z^{-4}$	$64.79\times Z^{-4}$
5	$1.314\times10^{-13}Z^{-5}$	$-50.85\times Z^{-5}$
6	$6.572\times10^{-14}Z^{-6}$	$24.94\times Z^{-6}$
7	$1.878\times10^{-14}Z^{-7}$	$-6.992\times Z^{-7}$
8	$2.347\times10^{-15}Z^{-8}$	$0.8575\times Z^{-8}$

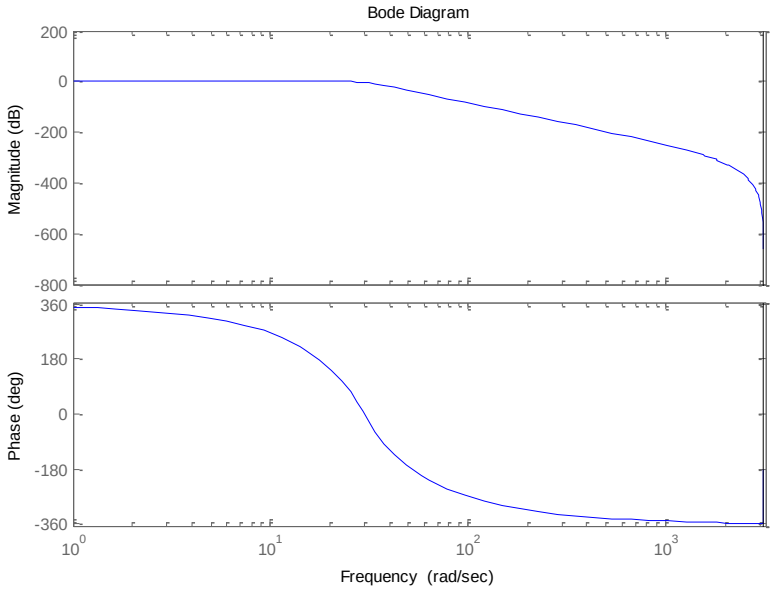

Figure 4-3: Butterworth filter's Bode plot.

The saturation function was used to limit the magnitude of the reference signal so that the amplified voltage is less than 4 V. This is to ensure the safe operation of dSPACE and to protect the programmable power supply. Because the programmable power supply can only amplify voltage emitted from dSPACE by four times, and the maximum voltage at which the programmable power supply can operate was 20 V.

As pointed out earlier, in this control approach, r = 0 functions as the sliding surface, on which the system is asymptotically stable, namely, the control error is zero. In order to force the system onto the sliding surface, we use the smooth robust controller $-\rho\tanh(\alpha r)$. The robust compensator was continuously differentiable with respect to the control variable r, and it generates a smooth control action (Song, et al., 2003).

Compared with the commonly used controllers such as bang–bang or saturation robust controllers, the robust controller has advantages in ensuring both smooth control input and eventually achieving identical global stability of the closed-loop system (Song, et al., 2003).

4.4 Experimental results

The defined controller was implemented in the Matlab/Simulink and dSPACE environment. The single SMA cable test frame was used for the experimental verification of the controller shown in equation 4-3.

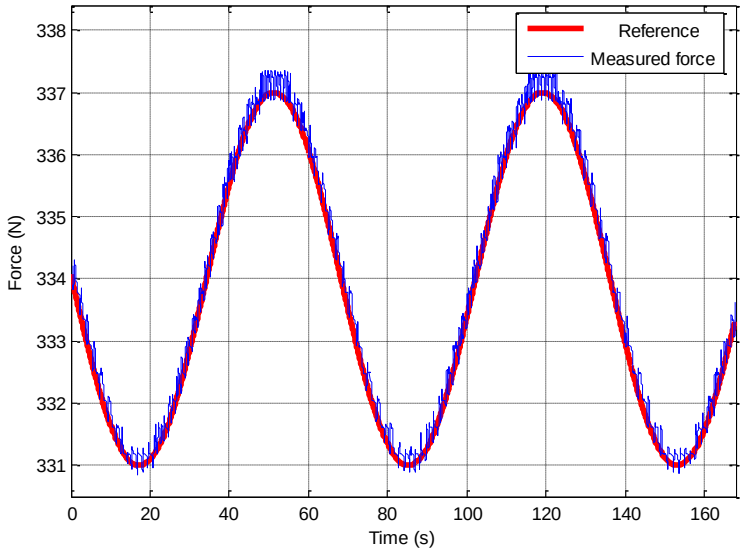

Figure 4-4: Sinusoid tracking control results.

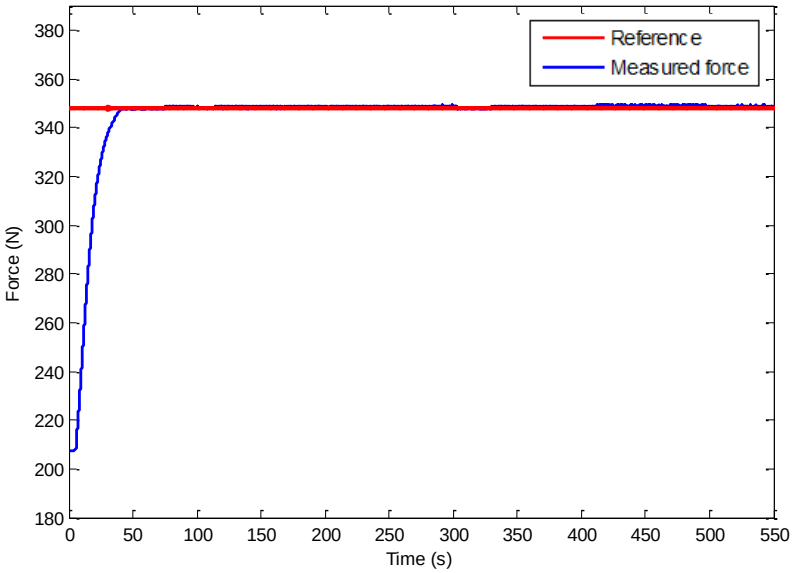

Figure 4-5: Constant force control results.

In order to simulate use in different applications, sinusoid and constant references were used. For the case of sinusoid, the controller parameters were λ=8, u_f=0.5, k=20, ρ=10, and α=10. For the case of constant force control the controller parameters were λ=8, u_f=0.49, k=20, ρ=10, and α=9.8.

The experimental results for the force of the SMA cable were shown in Figures 4-4 and 4-5. It can be clearly seen that the measured force of the SMA cable closely followed the reference signal. The transient performance was satisfactory and there was no overshoot. To better view the tracking performance of the SMA cable under the applied robust force controller, the force errors were plotted separately in Figures 4-6 and 4-7. The maximum sinusoid force tracking control error observed was 0.4 N, the Root-Mean-Square (RMS) error was 0.31 N. For the constant force control case, the maximum error observed was 0.1 N, and the RMS error was also 0.1 N. The constant force control had better accuracy than the sinusoid one, but their results were all very good. The applied voltages were shown in Figures 4-8 and 4-9.

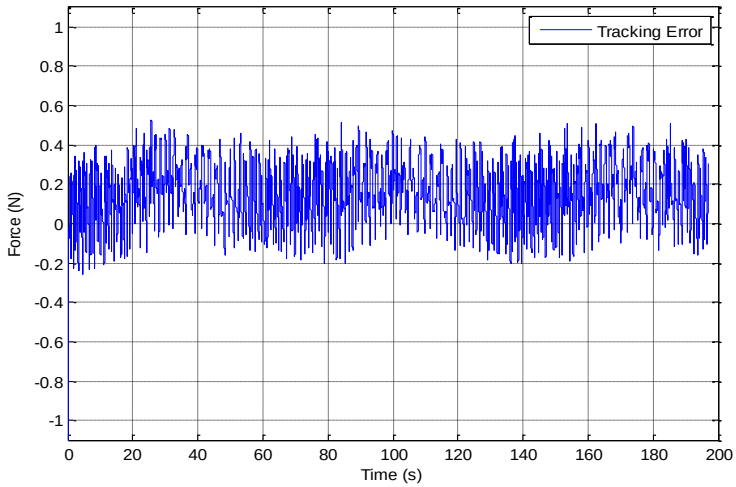

Figure 4-6: Force error for the sinusoid force tracking control.

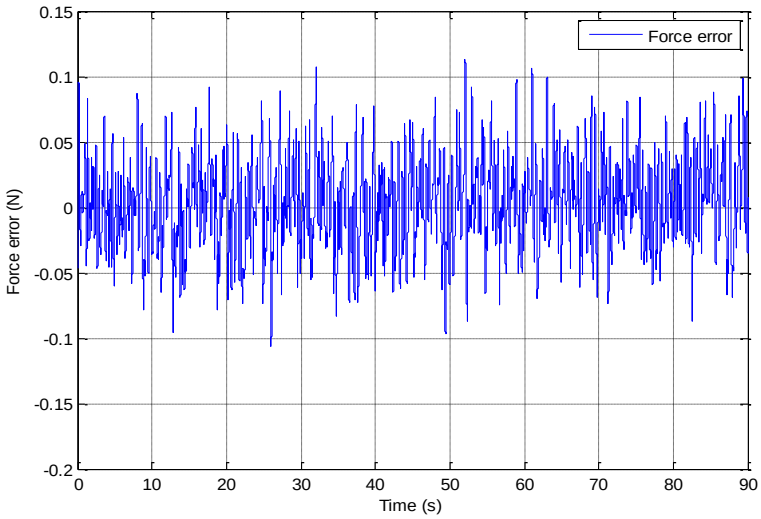

Figure 4-7: Force error for the constant force control.

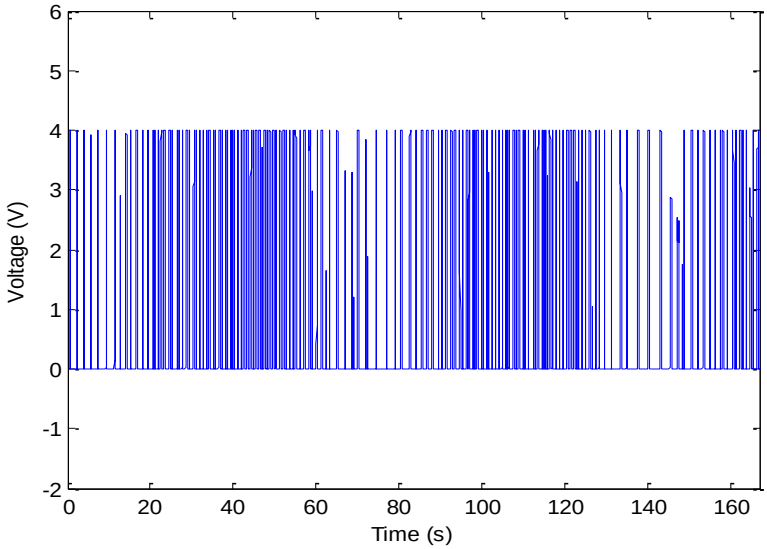

Figure 4-8: Applied voltage for the sinusoid force tracking control.

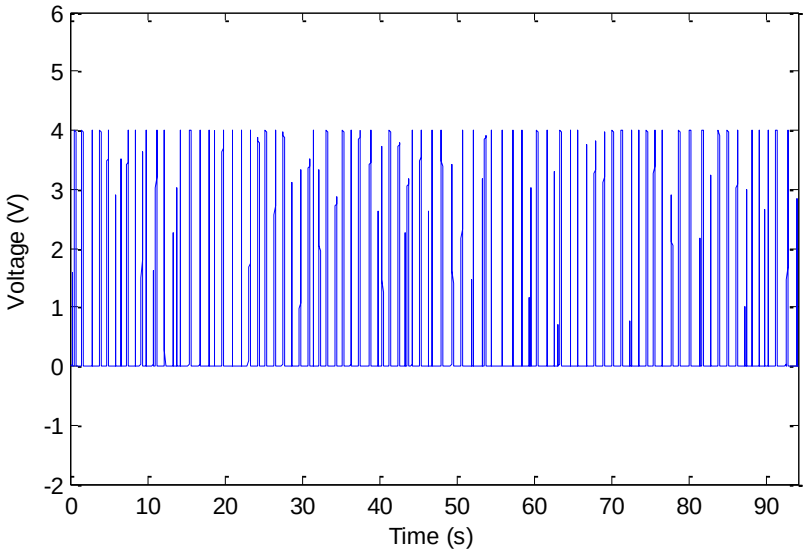

Figure 4-9: Applied voltage for the constant force control.

4.5 Summary

In this chapter, a sliding-mode based robust controller was conducted to control SMA cable with hysteresis compensation. The feedforward controller was used to cancel or reduce the hysteresis of the SMA cable and the sliding-mode based robust controller compensates uncertainties such as the error in hysteresis cancellation, while at the same time ensuring the system's stability. A single-cable SMA cable was used as the control object in this chapter. A testing system, which included a frame, a load cell, a programmable power supply, a personal computer (PC)-based digital data acquisition and real-time control system, were used to implement the conducted force controller. The experimental results show that the measured force of the cable closely followed that of the desired reference.

These results demonstrated that the conducted method of hysteresis compensation using a sliding-mode based controller was very effective. The following chapter stated methods used to take advantage of the constant force control in laboratory study.

Chapter 5 Application of control of shape memory alloy cables as reinforcement elements in engineered cementitious composite beams

5.1 Introduction

Research has been reported on SMA reinforced concrete. Kuang and Ou studied "passive smart self-repairing concrete beams by using shape memory alloy wires and fibers containing adhesives". They took advantage of the superelastic effect of SMA and the cohering characteristic of repairing adhesive (Kuang and Ou, 2008). Shrestha and co-authors investigated Cu-Al-Mn superelastic alloy bars as reinforcement elements in concrete beams to improve the self-repairing ability of concrete beams (Shrestha, et al., 2013). However, using SMA cables to improve the properties of engineered cementitious composite (ECC) beams has not been reported.

This study applies SMA cables as reinforcement elements in ECC beams, which is expected to improve ECC beams' load bearing capacity and to improve the self-repairing ability of the beam. In this chapter, shape memory effect (SME) of the superelastic Nitinol (SMA) cable was utilized when its temperature is below its martensite finish temperature. SMA can be easily deformed during the martensite phase (low temperature), and large restoring forces can be generated, if heated to austenite finish temperature, when encountering resistance, and this property can be used to post-tensioning the ECC beams. In this chapter, a sliding-mode based robust force controller was applied to control SMA cables, which was used to post-tensioning the ECC beams and also act as

reinforcement elements in the beams. Post-tensioned ECC beams will be experimentally studied to verify the increased load bearing and self-repairing capacities.

5.2 Experiment preparations

5.2.1 Casting of ECC beams

ECC beams with special sleeves have been cast and the size of the beams was 500× 50×25 mm. Also during the casting of the ECC beams, 7 sleeves were used, which reserved 7 conduits to thread 7 SMA cables through the beam, as shown in Figure 5-1.

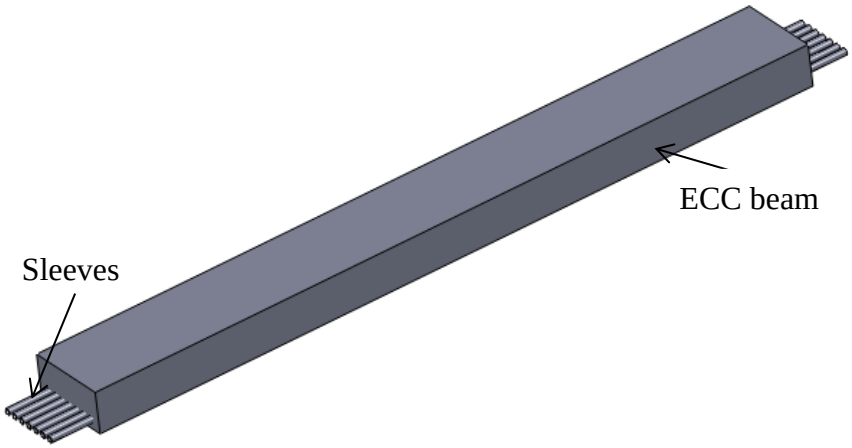

Figure 5-1: Schematic for the ECC beam with 7 sleeves.

5.2.2 Advantages of SMA cables

In this chapter, the Nitinol SMA cables were used. Nitinol has been proven to have following advantages; large recoverable strains, good electrical and mechanical properties, long fatigue life, good corrosion resistance, and high ultimate tensile strength (approximately 700 MPa).

5.3 Post-tensioning ECC using SME

5.3.1 Threading of SMA cables through ECC beams

With the sleeves, SMA cables were threaded through the ECC beam. In order to take advantage of the SME, as shown in Figure 5-2, the beam was placed in the freezer, which put the temperature of the SMA cables below its martensite finish temperature.

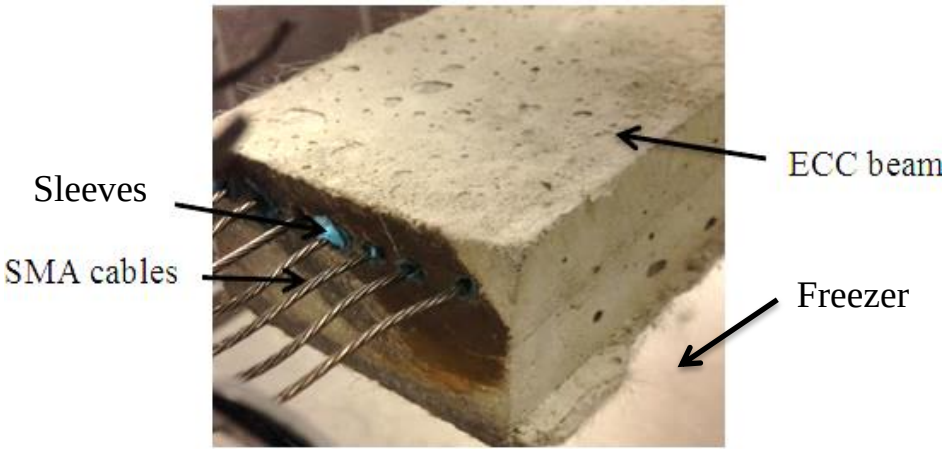

Figure 5-2: SMA cables were threaded through the ECC beams.

5.3.2 Connecting the ECC beam on the frame

As Figure 5-3 shows, the two ends of the SMA cables that run through the ECC beam were fixed on the frame. One end of beam was fixed on the frame through a hook while the other end was connected to the load cell, which was fixed on the frame. This setup allowed the force on the SMA cables to be measured.

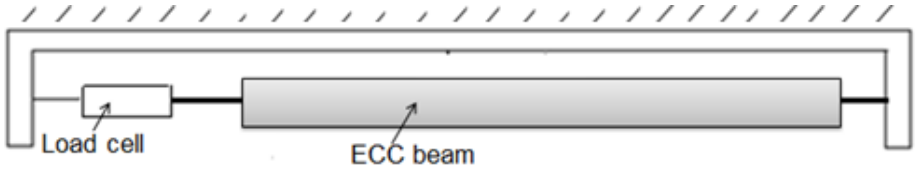

Figure 5-3: Schematic of connecting the ECC beam on the frame.

5.3.3 Force control of SMA cables to post-tensioning the ECC beam

In the freezer, the SMA cables were in their week martensite and were pre-tensioned by around 2% of its length. The control approach presented in Chapter 4 was used to control the SMA cables to achieve a desired force. This is to make sure that the SMA cables can enter an appropriate loading plateau with a pre-load force after they are brought into room temperature, when superelasticity occurs. Figure 5-4 shows the time history of the measured force with the force controller.

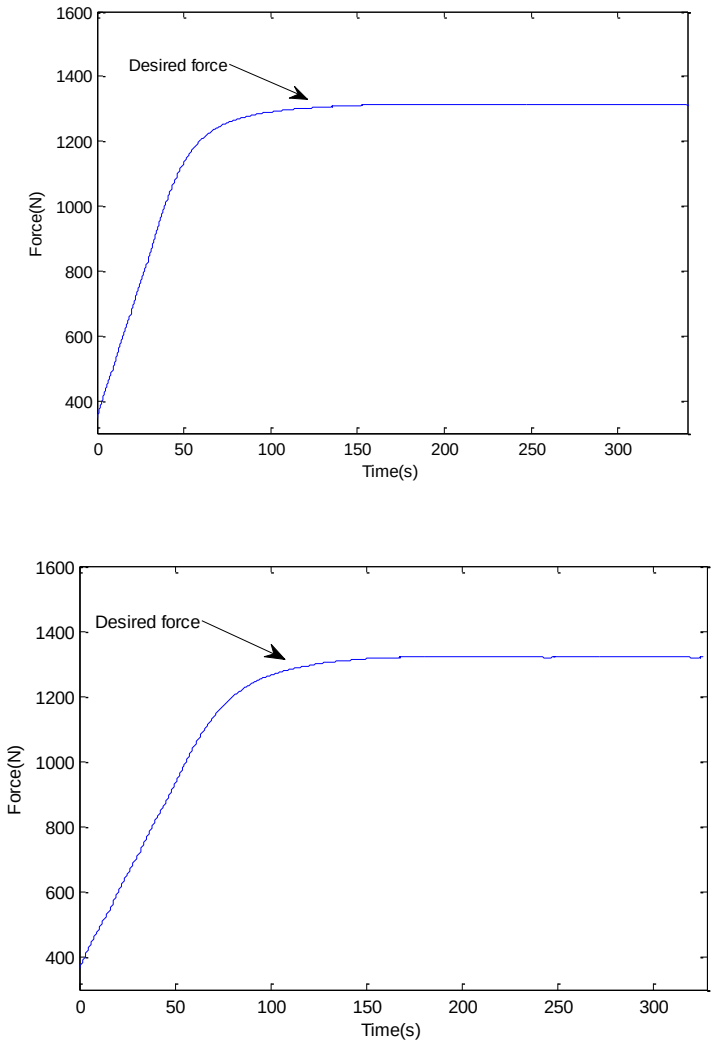

Figure 5-4: Force variation with controller in two repeated experiments.

5.3.4 Locking the post-tensioning force into ECC beam

After controlling the SMA cables to the desired force, specially designed clamps were used on each end of the SMA cables to lock the post-tensioning force into the ECC beam, which post-tensioned the ECC beam. As shown in Figure 5-5, the clamps were used to lock the force.

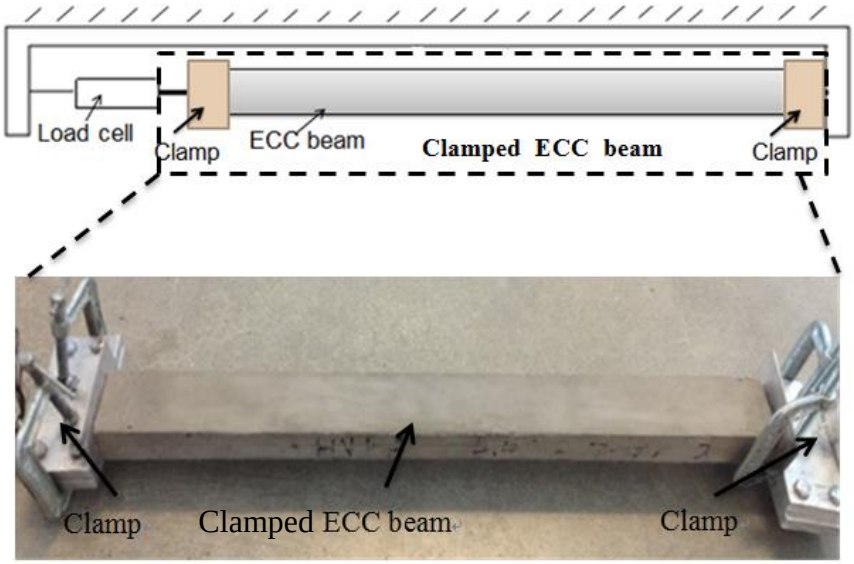

Figure 5-5: Schematic of using clamps to lock the post-tensioning force into the ECC beam.

5.3.5 Release the ECC beam

Then the ECC beam was disconnected from the frame and moved outside the freezer. The SMA cables eventually reached room temperature, which is above the austenite finish temperature of the SMA cables, and the SMA cables transformed to the austenite phase and exhibited superelasticity.

5.4 Experimental results on the post-tensioning force

5.4.1 Force remains after releasing of the ECC beam

As shown in Figure 5-6, two cases of the force history during the entire post-tensioning process were shown. After the SMA cable is controlled to a desired force

of 350 N, the power to the freezer is turn off and its cover is opened, followed by stopping the force controller. As soon as the electric current to the SMA cables were cut off, the cables returned to martensite since the temperature in the freezer was still low, and as a result, the cables loosened and the force dropped. The entire beam will reach room temperature gradually. As the temperature goes up to the room temperature, the SMA cables will change to the austenite phase, and, as a result, the SMA cables will contract and the force will go up again. In both cased, the final force was around 320 N, therefore, about 90.5 percent of the desired force was locked into the ECC beams. This means the proposed method to post-tensioning ECC beams was effective.

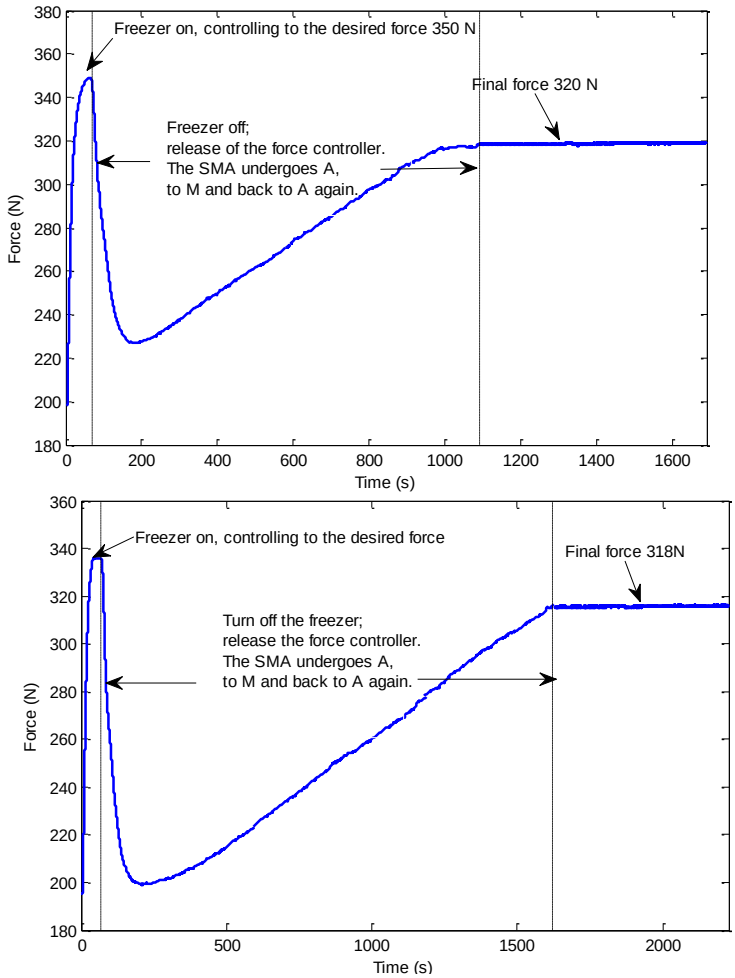

Figure 5-6: Force variation over time after releasing the force controller in two repeated experiments.

5.4.2 Force variation over temperature and pretension rate

Based on experimental results, the relationship of the force on the SMA cable with temperate and pretension rate is shown Figure 5-7.

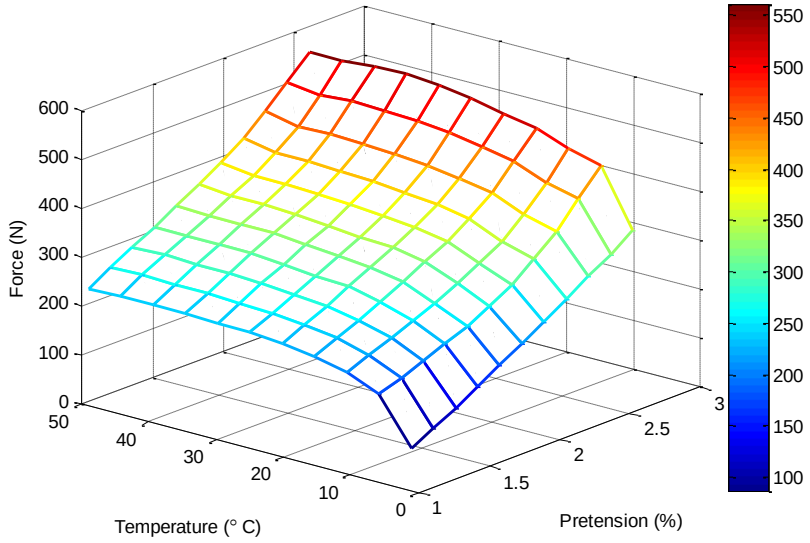

Figure 5-7: Force 3D-mapping over temperature and pretension.

5.5 Four-point loading and unloading tests under superelastic condition

The post-tensioned ECC beam was placed in the four-point test machine, as shown in Figure 5-8. The applied force and the deflection of the beam were recorded throughout the loading and unloading tests. The machine loaded the beam in an increment of 0.07 inch (1.778 mm) until failure was observed. At the end of each increment the beams was unloaded back to the original place. Thus for example the beam was loaded from 0 to 0.07 inch (1.778 mm), and then from 0 to 0.14 inch (3.556 mm) and so on until failure was observed. When the beam failed, both the beam and SMA cables were deformed significantly, and stress-induced martensite formed. When the test machine unloaded the beam, the martensite became unstable and the material returned to its original shape (austenite phase).

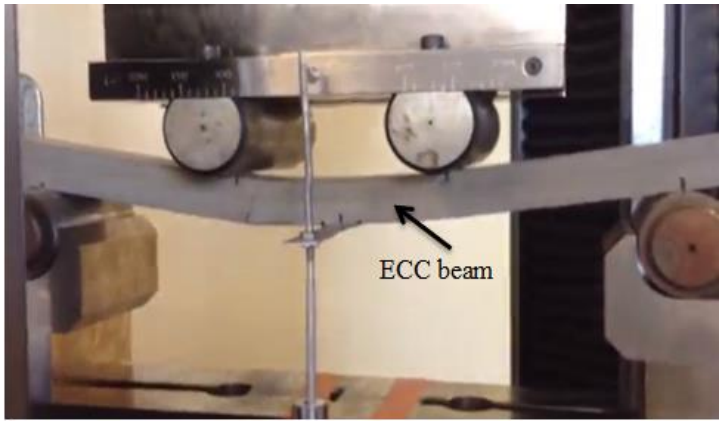

Figure 5-8: The four-point loading and unloading test (Provided by Xiaopeng Li and Mo Li, 2013).

5.6 Experimental results and discussion

In this chapter, both SME and superelasticity of SMA cables that reinforced the ECC beam were used. When its deflection reached 13.5 mm and the beam was bearing 1366 N, an average recovery of deflection of 90% was observed. The crack was significantly reduced and it could barely be seen by the naked eyes, as shown in Figure 5-9.

Figure 5-9: The crack before and after repairs.

By comparison, the ECC beam without post-tensioning had a load bearing capacity of 1103 N. This was observed when the deflection reached 17.2 mm. At this point the beam failed and an average recovery of deflection of 56% was observed.

From the results we can clearly see that the post-tensioned ECC beam with the Nitinol cables not only reduces cracking due to tensile stresses which occur due to externally applied tensile forces or bending moments but also improved the load bearing capacity. Furthermore, the superelasticity of SMA greatly helped the recovery of opened cracks.

Table 5-1: Comparison with and without post-tensioned ECC beams.

Parameters	With SMA reinforced	Without SMA reinforced
Maximum deflection	13.5 mm	17.2 mm
Maximum bearing force	1366 N	1103 N
Cracks recovery	90%	56%

5.7 Summary

This chapter reports the innovative work of improving engineered cementitious composite beams using superelastic Nitinol shape memory alloy (SMA) cables. Firstly, by applying the Nitinol cables as reinforcement elements in the ECC beams, although large deflection or cracks happened after loading the ECC beams, deflection or cracks can almost completely recovery. Secondly, increasing the numbers of Nitinol cables can effectively increase the load bearing capacity and stiffness of the ECC beams without sacrificing the beams' ductility. Thirdly, post-tensioned ECC beams can reduce the crack width. Lastly, compared with normal concrete beams reinforced with SMA cables, the Nitinol reinforced ECC beam has better self-repairing capacity after the crack occurs.

Chapter 6 Conclusions and future work

6.1 Conclusions

This thesis reports the innovative work of improving engineered cementitious composite (ECC) beams using superelastic Nitinol shape memory alloy (SMA) cables. To understand the characteristics of the Nitinol cable, a series of experiments were conducted to derive its key parameters, which were not provided by the manufacturer. A sliding mode based robust controller was designed and tested to ensure the accurate force control of the Nitinol cable during the process of post-tensioning of the ECC beam. In this research, the shape memory effect (SME) of the same superelastic Nitinol cable when its temperature was below its martensite finish temperature was used to post-tensioning the ECC beam with a pre-loaded force. Experiments demonstrated that the ECC reinforced with the superelastic Nitinol cable with a pre-loaded force greatly increases the load bearing and self-repairing capacities of the ECC beam without sacrificing its ductility.

6.2 Future work

Although the approach in this thesis can obtain the characteristics of SMAs, for example, the transformation temperatures. The ambient temperature changes can adversely affect the results, especially when the entire test was conducted in a freezer whose temperature cannot be precisely controlled. Future work will involve how to address this problem, an approach can be the use of a feedback control to accurate control the temperature of the SMA cable. Additional approach can be the use of the method of differential scanning calorimetry (DSC) to measure the transformation temperatures for comparison purposes.

A sliding-mode based robust controller was used successfully for force tracking of the SMA cables. However, in order to achieve the goal, a programmable power supply was needed, which was relatively expensive and increased the cost. Future work will use a pulse-width modulation (PWM) modulated sliding-mode based robust controller or other controllers with a regular constant voltage power supply instead of a programmable power supply.

SMA reinforced ECC beams with post-tensioning improved the self-repairing ability and load bearing capacity of the ECC beams. It is believed that the SMA cables can increase the damping capacity of the ECC beams. Future work will also involve experimental validation of this.

Prestressed concrete has been utilized and came into service for more than one century. It can reduce or even eliminates cracks due to tensile stresses which occur due to externally applied tensile forces or bending moments (Moser, et al., 2005). This is one of the major reasons for used of prestressed concrete. This research only studied ECC beams with post-tensioned SMA cables. Future study will involve prestressed SMA cables.

References

Brinson L.C., (1993). "One-dimensional Constitutive Behavior of Shape Memory Alloys: Thermomechanical Derivation with Non-constant Materials Functions and Redefined Martensite Internal Variable." *Journal of Intelligent Materials Systems and Structures*. **4**: 229-242

Choon T.W., Salleh A.S. and Jamian S., (2007). "Phase Transformation Temperature for Shape Memory Alloy Cable." *World Academy of Science, Engineering and Technology*. **25**: 304-307

Desroches R., McCormick J. and Delemont M., (2004). "Cyclic Properties of Superelastic Shape Memory Alloy Wires and Bars." *Journal of Structural Engineering*. **38**: 38-46

Elahinia M.H. and Ahmadian M., (2005). "An Enhanced SMA Phenomenological Model: II. The Experimental Study. " *Smart materials and structures*. **14**: 01-06

Furukawa T.M., (2001). "Shape Memory Alloys and Super-elastic Alloys." from https://www.furukawa-ftm.com/english/nt-e/actuator01.htm

Hodgson D.E., Wu M.H. and Biermann R.J., (2002). "Shape Memory Alloys." from http://heim.ifi.uio.no/~mes/inf1400/COOL/Robot%20Prosjekt/Flexinol/Shape%20Memory%20Alloys.htm

Inamura T., Hosoda T., Wakashima K. and Miyazaki S., (2005). "Anisotropy and Temperature Dependence of Young's Modulus in Textured TiNbAl Biomedical Shape Memory Alloy." *Materials Transactions*. **46**: 1597-1603

Kim K., (2002). "Fatigue Properties of the Ti-Ni Base Shape Memory Alloy Cable." *Japan Institute of Materials*. **43**: 1703-1706

Kotil T., Sehitoglu H., Maier H.J. and Chumlyakov Y.I., (2003). "Transformation and detwinning induced electrical resistance variations in NiTiCu." *Materials Science and Engineering.* **A359**: 280-289

Kuang Y.C. and Ou J.P., (2008). "Passive Smart Self-repairing Concrete Beams by Using Shape Memory Alloy Cables and Fibers Containing Adhesives." *Journal of Center South University Technology.* **15**: 411-417

Li P., (2011). "Low Power Piezoceramic Based Cableless Sensor Networks for Structural Monitoring and Controls and a Real Time Embedded System for Advanced Controls." *Doctor's desertion, University of Houston*

Li V.C., (2013). "Effect of Concrete Material Ductility on the Damage Mechanisms and Processes in Steel/Concrete Interaction Zones." from http://ace-mrl.engin.umich.edu/NewFiles/projects/Interaction.html

Li V.C. and Kanda T., (1998). "Engineered Cementitious Composites for Structural Application." *Department of Civil and Environmental engineering University of Michigan*. **2**: 66-69

Liu S.H., Huang T.S. and Yen J.Y., (2010). "Tracking Control of Shape Memory Alloy Actuators Based on Self-Sensing Feedback and Inverse Hysteresis Compensation." *Sensors*. **10**: 112-127

Loh C.S., Yokoi H., and Arai T., (2005). "New Shape Memory Alloy Actuator: Design and Application in the Prosthetic Hand." *Proceedings of the IEEE Engineering in Medicine and Biology 27th Annual Conference.* 6900-6903

Ma N. and Song G., (2003). "Control of Shape Memory Alloy Actuator Using Pulse Width Modulation." *Smart Materials and Structures.* **12**: 712-719

Ma N., Song G. and Lee H.J., (2004). "Position Control of Shape Memory Alloy Actuators with Internal Electrical Resistance Feedback Using Neural Networks." *Smart Materials and Structures.* **13**: 777-783

Moser K., Bergamini A., Christen R. and Czaderski C., (2005). "Feasibility of Concrete Prestressed by Shape Memory Alloy Short Fibers." *Materials and Structures*. **38**: 593-600

Nguyen B.K., Nguyen D.T. and Kyoung K.A., (2007). "Hysteresis Compensation for Shape Memory Alloy Actuators Using a Fuzzy Based Inverse Preisach Model." *International Symposium on Electrical & Electronics Engineering*. 92-97

Orvis S.M., (2009). "Prestress Concrete with Shape Memory Alloy Fibers." A Thesis, *California Polytechnic State University*

Shrestha K.C., Araki Y., Nagae T. and Koetaka Y., (2013). "Feasibility of Cu-Al-Mn Superelastic Alloy Bars as Reinforcement Elements in Concrete Beams." *Smart Materials and Structures*. **22**: 025025

Song G., (2013). "Intelligent Structural Systems" Class Notes, *Department of Mechanical Engineering, University of Houston*

Song G., Chaudhry V. and Batur C., (2003). "Precision Tracking Control of Shape Memory Alloy Actuators Using Neural Networks and a Sliding-mode Based Robust Controller." *Smart Materials and Structures*. **12**: 223-231

Song G., Kelly B. and Agrawal B.N., (2000). "Active Position Control of A Shape Memory Alloy Wire Actuated Composite Beam." *Smart Materials and Structures*. **9**: 711-716

Song G. and Ma N., (2007). "Robust Control of a Shape Memory Alloy Wire Actuated Flap." *Smart Materials and Structures*. **16**: N51-N57

Song G., Ma N., Li H.N., (2006). "Application of Shape Memory Alloys in Civil Structures." *Engineering structures*. **28**: 1266-1274

Sreekala R., Muthumani K. and Nagesh R.I., (2011) "Seismic Response Control Using Smart Materials." *InTech*. **9**: 173-196

Swamy R., Prashantha S. and Mallikarjun, (2012). "Characterization of Cu-Al-Be Shape Memory Alloys." IOSR *Journal of Mechanical and Civil Engineering*. 01-06

Uchil J., (2002). "Shape Memory Alloys-Characterization Techniques." *Journal of physics Indian Academy of Sciences*. **58**: 1131-1139

Wu M.H. and Schetky L.M., (2000). "Industrial Applications for Shape Memory Alloys." *Proceedings of the International Conference on Shape Memory and Superelastic Technologies*. 171-182

Zak A.J., Cartmell M.P., Ostachowicz W.M. and Wiercigroch M., (2003). "One-Dimensional Shape Memory Alloy Models for Use with Reinforced Composite Structures." *Smart Materials and Structures*. **12**: 338-346